

THESIS

A NOVEL DIRECT SHEAR APPARATUS TO EVALUATE INTERNAL SHEAR STRENGTH OF  
GEOSYNTHETIC CLAY LINERS FOR MINING APPLICATIONS

Submitted by

Mohammad R. Soleimanian

Department of Civil and Environmental Engineering

In partial fulfillment of the requirements

For the Degree of Master of Science

Colorado State University

Fort Collins, Colorado

Fall 2016

Master's Committee:

Advisor: Christopher A. Bareither

Charles D. Shackelford

Steven L. Schaeffer

Copyright by Mohammad R. Soleimani 2016

All Rights Reserved

## ABSTRACT

### A NOVEL DIRECT SHEAR APPARATUS TO EVALUATE INTERNAL SHEAR STRENGTH OF GEOSYNTHETIC CLAY LINERS FOR MINING APPLICATIONS

The use of geosynthetic clay liners (GCLs) in engineering practice has grown extensively over the past three decades due to application of this material containment applications such non-hazardous solid waste, residential and commercial wastewater management, roadways, and other civil engineering construction projects. This growth has been supported by an enhanced understanding of the engineering properties of GCL as well as hydraulic and mechanical behavior for different applications. In particular, the internal shear strength of GCLs is an important design consideration since GCLs often are installed on sloped surfaces that induced internal shear and normal stresses.

The objective of this study was to develop a direct shear testing apparatus to measure the internal shear strength of GCLs for use in mining applications. The direct shear apparatus was designed to support the following testing conditions for needle-punched reinforced GCLs: hydration and testing in non-standard solutions (e.g.,  $\text{pH} \leq 1$  or  $\text{pH} \geq 12$ ); testing under high normal stresses (up to 2000 kPa); and testing at elevated temperatures (up to 80 °C). Ultra-high molecular weight polyethylene GCL shear boxes were developed to facilitate testing 300-mm-square and 150-mm-square specimens under displacement-controlled conditions. Experiments were conducted on 150-mm-square and 300-mm-square GCL specimens to (i) evaluate gripping surface effectiveness as a function of peel strength and normal stress, (ii) assess hydration procedures to adopt into a systematic shear-testing protocol, (iii) assess stress-displacement behavior for 150-mm and 300-mm GCL shear tests, and (iv) develop failure envelopes for peak shear strength ( $\tau_p$ ) and large-displacement ( $\tau_{ld}$ ).

Shear behavior and peak and large-displacement shear strengths measured on both 150-mm and 300-mm square GCL specimens compared favorably to one another as well as to data from a previous study on a similar GCL. These comparisons validated the direct shear apparatus developed in this study and support the use of small GCL test specimens to measure internal shear behavior and shear strength of reinforced GCLs. Furthermore, the pyramid-tooth gripping plates developed to transfer shear stress from the interfaces between geotextiles of the GCL and shear platens to the internal region of a GCL were effective for a needle-punched GCL with peel strength of 2170 N/m and at normal stress  $\geq 100$  kPa.

## ACKNOWLEDGEMENTS

I would like to express thanks to my committee members, Dr. Charles Shackelford and Dr. Steven Schaeffer, and especially my adviser Dr. Christopher Bareither who continuously supported me throughout this program. Also, I would like to express a special thanks to both Dr. Steven Schaeffer and Joe Wilmetti for their help on all aspects of design, construction, and maintenance of the direct shear apparatus. Completion of this project would not have been possible with their endless contributions.

I appreciate the support of my classmates, lab-mates, and office-mates: Aliena Debelak, Sultan Alhomair, Mohammad Reza Gorakhki, Shahin Ghazizadeh, Zhengguang Tian, Shan Tong, Kelechi Nwaokorie, and specifically Matteus Hamade who tirelessly helped me with developing the apparatus. I am grateful for spending time side-by-side with all of you.

Words cannot express the thanks I send to my parents: Mohammad and Sima for supporting me without any hesitation. Reaching this milestone in my life was not achievable without their support. And at last but not least, I want to thank my fiancé, Ferial, for her patience during this long time that I spent away from her.

Financial support for this study was provided by Colorado State University, the Tailings and Mine Waste Conference Committee, and CETCO/Minerals Technology, Inc. I am grateful for all of their contributions to make this project successful.

## TABLE OF CONTENTS

ABSTRACT.....	ii
ACKNOWLEDGEMENTS .....	iv
LIST OF TABLES.....	vii
LIST OF FIGURES .....	viii
CHAPTER 1: INTRODUCTION.....	1
1.1 Problem Statement.....	1
1.2 Research Objectives and Tasks .....	3
CHAPTER 2: BACKGROUND .....	6
2.1 Geosynthetic Clay Liners.....	6
2.1.1 Brief History .....	6
2.1.2 Type of Geosynthetic Clay Liners.....	7
2.2 Field-Scale Testing of Geosynthetic Clay Liners.....	8
2.3 Laboratory-Scale Testing of Geosynthetic Clay Liners.....	9
2.3.1 Shear Strength Testing .....	9
2.3.2 Analysis of Shear Behavior and Shear Strength.....	10
2.3.2.1. Shear Stress versus Horizontal Displacement .....	10
2.3.2.2. Failure Envelopes for Needle-Punched GCLs.....	11
2.4 Factors Affecting Shear Behavior and Strength of GCLs .....	12
2.4.1 Manufactured Properties of GCLs .....	13
2.4.1.1 Type of Reinforcement .....	13
2.4.1.2 Reinforcement Fibers and GCL Peel Strength .....	14
2.4.1.3 Thermal-Bonding of Reinforcement Fibers. ....	15
2.4.2 Shear Testing Conditions of Geosynthetic Clay Liners.....	15
2.4.2.1 Hydration and Consolidation.....	15
2.4.2.2 Normal Stress.....	18
2.4.2.3 Geotextile Gripping and Clamping. ....	18
2.4.2.4 Shear Displacement Rate. ....	19
2.4.2.5 Temperature .....	20
CHAPTER 3: METHODS AND MATERIALS.....	35
3.1 Direct Shear Apparatus .....	35

3.1.1 Normal Force Loading System .....	35
3.1.2 Shear Force Loading System .....	35
3.1.3. External Shear Box .....	37
3.1.4. Internal GCL Shear Boxes .....	37
3.1.5. Data Acquisition and Control System .....	40
3.2. Materials .....	41
3.3 Testing Procedure .....	42
3.3.1. Specimen Cutting .....	42
3.3.2 Specimen Hydration .....	42
3.3.3. GCL Shear Testing .....	43
CHAPTER 4: RESULTS AND DISCUSSION .....	54
4.1. Effectiveness of the Pyramid-Tooth Gripping Plates .....	54
4.1.1 Influence of Normal Stress .....	54
4.1.2. Influence of GCL Peel Strength .....	55
4.2. Evaluation of Hydration Procedure .....	56
4.3. Shear Plane Area Correction .....	57
4.4. Shear Stress-Displacement Relationships and Failure Envelopes .....	59
CHAPTER 5: CONCLUSIONS AND FUTURE WORK .....	70
5.1 Conclusions .....	70
5.2 Future Work .....	71
REFERENCES .....	72

## LIST OF TABLES

Table 2.1. Direct shear tests on internal shear strength of needle-punched reinforced geosynthetic clay liners. ....	21
Table 2.2. Direct shear testing summary from Fox et al. (1998). ....	23
Table 2.3. Description of shear platen gripping surfaces used in Allen and Fox (2007) to transfer shear force from shear platen onto the surface of the GCL during shear testing. ....	24
Table 3.1. Summary of geosynthetic clay liner material characteristics. ....	46
Table 3.2. Summary of shear tests conducted to evaluate the GCL hydration procedure. ....	47
Table 3.3. Summary of shear tests conducted to evaluate repeatability ....	48
Table 4.1. Summary of geosynthetic clay liner direct shear experiments conducted as part of this study to evaluate internal shear strength. ....	63



## LIST OF FIGURES

Fig. 1.1. Cross-sectional schematic of a heap leach facility.....	5
Fig. 2.1. Schematics of dry (a) needle-punched and (b) stitch-bonded internally-reinforced geosynthetic clay liners .....	25
Fig. 2.2. Cross-section of an 3H:1V test plot constructed to evaluate interface/internal slope stability of cover systems employing a geosynthetic clay liner (Daniel et al. 1998). .....	26
Fig. 2.3. Schematics of shear testing apparatuses: (a) direct shear, (b) ring shear, and (c) inclined plane shear (Not to scale).....	27
Fig. 2.4. Typical shear stress versus horizontal displacement relationship for internal shear strength testing of reinforced geosynthetic clay liners.....	28
Fig. 2.5. Example of typical failure envelopes to define shear strength parameters (Fox and Stark 2004). .....	29
Fig. 2.6. Failure envelopes for peak and residual shear strength from Fox et al. (1998). Note: GCL-1 = unreinforced GCL, GCL-2 = stitch-bonded GCL, and GCL-3 = needle-punched GCL.....	30
Fig. 2.7. Relationships of peak shear strength versus normal stress for a needle-punched reinforced geosynthetic clay liner (i.e., Bentomat ST) manufactured with a range of peel strengths (PS). References: 1 = Fox et al. (1998), 2 = Zornberg et al. (2005), and 3 = Athanassopoulou and Yuan (2011). .....	31
Fig. 2.8. Effect of consolidation on internal peak shear strength of a needle-punched reinforced geosynthetic clay liner (McCartney et al. 2009). .....	32
Fig. 2.9. Shear stress-displacement relationships from Allen and Fox (2007) for evaluation of different gripping surfaces. Experiments performed under (a) $\sigma_n = 9.6$ kPa, (b) $\sigma_n = 48$ kPa , and (c) $\sigma_n = 480$ kPa.....	33
Fig. 2.10. Relationships of peak shear strength versus displacement rate for ring shear tests conducted on a thermally-bonded, needle-punched reinforced geosynthetic clay liner (Eid et al. 1999).....	34
Fig. 3.1. Cross-section (a) and plan-view (b) schematics of the direct shear apparatus. ....	49
Fig. 3.2. Picture of direct shear apparatus with data acquisition system and personal computer.....	50
Fig. 3.3. Cross-section schematic of the 300-mm-square internal shear box that is positioned inside the external shear box for shear testing. Notes: GCL = geosynthetic clay liner; UHMW = ultra-high molecular weight polyethylene. ....	51

Fig. 3.4. Temporal relationships of temperature within the hydration solution and within the bentonite clay layer of a GCL for the following experiments: (a) 300-mm GCL heated to ~ 50 °C; (b) 150 -mm GCL heated to ~ 50 °C; (c) 300 -mm GCL heated to ~ 80 °C; and (d) 150-mm GCL heated to ~ 80 °C. ....	52
Fig 16 Relationships of shear stress versus horizontal displacement for two sets of experiments conducted to evaluate repeatability. Hydration conditions for these experiments are summarized in Table 3.3, and all experiments were conducted on 150-mm-square specimens of GCL-A at a normal stress of 100 kPa. ....	53
Fig. 4.1. Relationships of shear stress versus horizontal displacement for 150-mm-square GCL specimens conducted to evaluate the effectiveness of the pyramid-tooth plates versus (a) normal stress and (b) peel strength of specimen.....	64
Fig. 4.2. Relationships of shear stress versus horizontal displacement for 150-mm-square GCL specimens conducted to evaluate 2-step hydration procedures. ....	65
Fig. 4.3. Relationships of shear stress and normal stress versus horizontal displacement for considerations of no-area correction applied during shear and corrected shear and normal stress based on a reducing shear plane area. Example data are shown for a direct shear test conducted on a 150-mm specimen. ....	66
Fig. 4.4. Relationships of shear stress and net vertical displacement versus horizontal displacement for shear tests conducted: (a) shear stress for 150-mm specimens, (b) shear stress for 300-mm specimens, (c) vertical displacement for 150-mm specimens, and (d) vertical displacement for 300-mm specimens.....	67
Fig. 4.5. Peak and large-displacement failure envelopes for the needle-punched reinforced GCL tested in this study. Data from Fox and Ross (2011) are for a comparable GCL. Failure envelopes shown in the plot: (i) bilinear, peak shear strength failure envelope for 150- and 300-mm GCL tests with one failure envelope for $\sigma_n \leq 500$ kPa and one for $\sigma_n \geq 500$ ; (ii) nonlinear, peak shear strength failure envelope for 150-mm and 300-mm GCL tests; (iii) linear, large-displacement shear strength failure envelope for 150-mm GCL shear tests based on shear stress at horizontal displacement = 70 mm; and (iv) linear, large-displacement shear strength failure envelope for 300-mm GCL shear tests based on shear stress at horizontal displacement = 100 mm large-displacement shear strengths. ....	68
Fig. 4.6. Relationships of displacement to peak shear stress versus normal stress for shear tests conducted on 150-mm and 300-mm specimens.....	69

## **CHAPTER 1: INTRODUCTION**

Geosynthetic clay liners are a manufactured product used as a hydraulic barrier for applications such as waste containment systems, surface impoundments, storage tanks, canals, and heap leach ponds (Koerner 1998). Geosynthetic clay liners typically consist of a layer of sodium bentonite sandwiched between two geotextiles (GT) or adhered to a geomembrane (GM). Sodium bentonite swells when exposed to water to create a low hydraulic conductivity layer that makes GCLs effective components of hydraulic barrier systems. Geosynthetic clay liners have gained increasing use in geotechnical engineering since the 1980s due to numerous advantages; e.g., low hydraulic conductivity, competitive costs to other design alternatives, ease of handling and installation, reduced volume requirements, self-healing of hydraulic resistance, and effectiveness against freeze/thaw cycles (Koerner 1997; Bouazza 2002).

### **1.1 Problem Statement**

Mining operations are increasingly targeting lower-grade ore bodies for metal extraction. An effective method for liberating metals from low-grade ore is heap leaching (Fig. 1.1), which has been used to recover gold, copper, silver, uranium, and nickel. Heap leaching is a technique whereby a lixiviant, or leach solution, is introduced to a pile of crushed ore, the lixiviant flows through the ore and dissolves metals into solution, and the pregnant leach solutions (PLS) that contains solubilized metals is transferred along the liner system of a leach pad to a collection pond (Fig. 1.1) (Theil and Smith 2004; Lupo 2010). The liner system of a heap leach pad is a critical part of the engineering design such that the PLS is collected for subsequent metallurgical processing and does not leak into the environment. Liner systems are routinely constructed with natural or geosynthetic materials; however, the use of GCLs in liner systems for heap leach pads has gained relatively little traction due primarily to concerns of

short- and long-term GCL shear strength in the presence of high stresses, non-standard solutions, and elevated temperatures (Theil and Smith 2004; Horsney et al. 2010; Lupo 2010).

Shear strength of GCLs is a critical design consideration as GCLs are commonly used on slopes that induce shear stresses on the surface of the GCL (interface) and within the GCL (internal). Internal shear strength of GCLs is particularly important considering Gleason et al. (1997) reported an internal friction angle of sodium bentonite equal to 12° and hydrated sodium-montmorillonite (i.e., primary mineral in bentonite clay) can have internal friction angles as low as 0° to 4° (Mesri and Olson 1970). The internal shear strength of GCLs can be increased above the frictional angle of hydrated sodium bentonite via stitch-bonding or needle-punching the carrier and cover geotextiles together to create internal reinforcement.

The range of normal stresses ( $\sigma_n$ ) used to assess GCL shear strength depends on the intended application; e.g., low  $\sigma_n$  (10 to 50 kPa) is relevant to cover systems, whereas higher  $\sigma_n$  (500 to > 2000 kPa) is relevant to liner systems in landfills and heap leach pads. An increase in peak and large-displacement shear strength coincides with increasing shearing  $\sigma_n$  such that internal failure of GCLs exhibit frictional behavior and failure criteria can be defined via linear and nonlinear failure envelopes (Fox and Stark 2015). Fox and Ross (2011) reported a transition from interface failure between a textured geomembrane and needle-punched GCL for  $\sigma_n < 1380$  kPa to partial interface / internal GCL failure for  $\sigma_n$  between 1380 kPa and 2070 kPa, and complete internal GCL failure for  $\sigma_n > 2070$  kPa. This transition in complete internal failure at high  $\sigma_n$  supports the importance of internal GCL shear strength for high  $\sigma_n$  applications.

Exothermic chemical and biological reactions in heap leach facilities can lead to elevated temperatures on liner systems (e.g., Smith 2008), whereas elevated temperatures in cover systems are a function on geographic location and climatic fluctuations (Koerner and Koerner 2006; Hanson et al. 2010). Temperatures of 45 °C have been reported in copper sulfide leaching and 75 °C in nickel leaching, which can affect geosynthetic properties (Smith 2008). In

addition, GCLs used in liner systems for heap leach facilities can be exposed to a broad range of inorganic chemical solutions that can influence polymer degradation (e.g., Bouazza 2002; Hornsey et al. 2010). For example, Hsuan (2002) reported that the type and abundance of antioxidants in polymer-based geosynthetics are the primary factors controlling resistance against long-term oxidative degradation. Antioxidants in all polymeric geosynthetics are reduced during the lifespan of the geosynthetics, and the rate of antioxidant depletion increases with increasing temperature and/or increasing oxygen concentration (Hsuan 2002). Hornsey et al. (2010) reported that the combination of strongly acidic or alkaline mine process waters with elevated temperature represent critical conditions to long-term geosynthetic performance in mining applications.

## **1.2 Research Objectives and Tasks**

The objective of this study was to develop a direct shear apparatus capable of performing shear strength experiments on GCLs exposed to mine solutions (e.g.,  $\text{pH} \leq 1$  to  $\text{pH} \geq 12$ ), high normal stresses ( $\sigma_n \approx 2000$  kPa) and elevated temperatures (up to  $80$  °C). The following research tasks were completed as part of this study:

1. Design and construct the new direct shear apparatus;
2. Evaluate functionality of conducting internal direct shear experiments on GCLs;
3. Evaluate a gripping and clamping system GCL shear testing that (i) yields effective internal failure for GCLs tested at low  $\sigma_n$  and (ii) yields effective internal failure of GCLs with different peel strengths;
4. Evaluate shear behavior (i.e., shear stress and vertical displacement versus horizontal displacement) for 150-mm-square GCL test specimens at  $\sigma_n$  ranging from 100 to 2000 kPa and for 300-mm-square GCL test specimens at  $\sigma_n$  ranging from 100 to 500 kPa; and

5. Create failure envelopes for internal peak and large-displacement shear strength and compare with previous studies to validate the new direct shear apparatus.

A detailed description of the direct shear apparatus and functionality of the apparatus with respect to  $\sigma_n$  and elevated temperature is documented herein. An assessment of the gripping and clamping system was conducted via (i) testing a single type of GCL at  $\sigma_n = 20, 50, 80,$  and  $100$  kPa, and (ii) testing three different GCLs with peel strengths approximately equal to  $1400, 2170,$  and  $2600$  N/m under the same  $\sigma_n$ . Failure envelopes for peak and large-displacement shear strength were created from eight direct shear experiments, which included three tests on 300-mm-square specimens and five tests on 150-mm-square GCL specimens. Failure envelopes presented from Fox and Ross (2011) for a similar NP-GCL were compared to failure envelopes developed in this study to validate functionality of the apparatus.

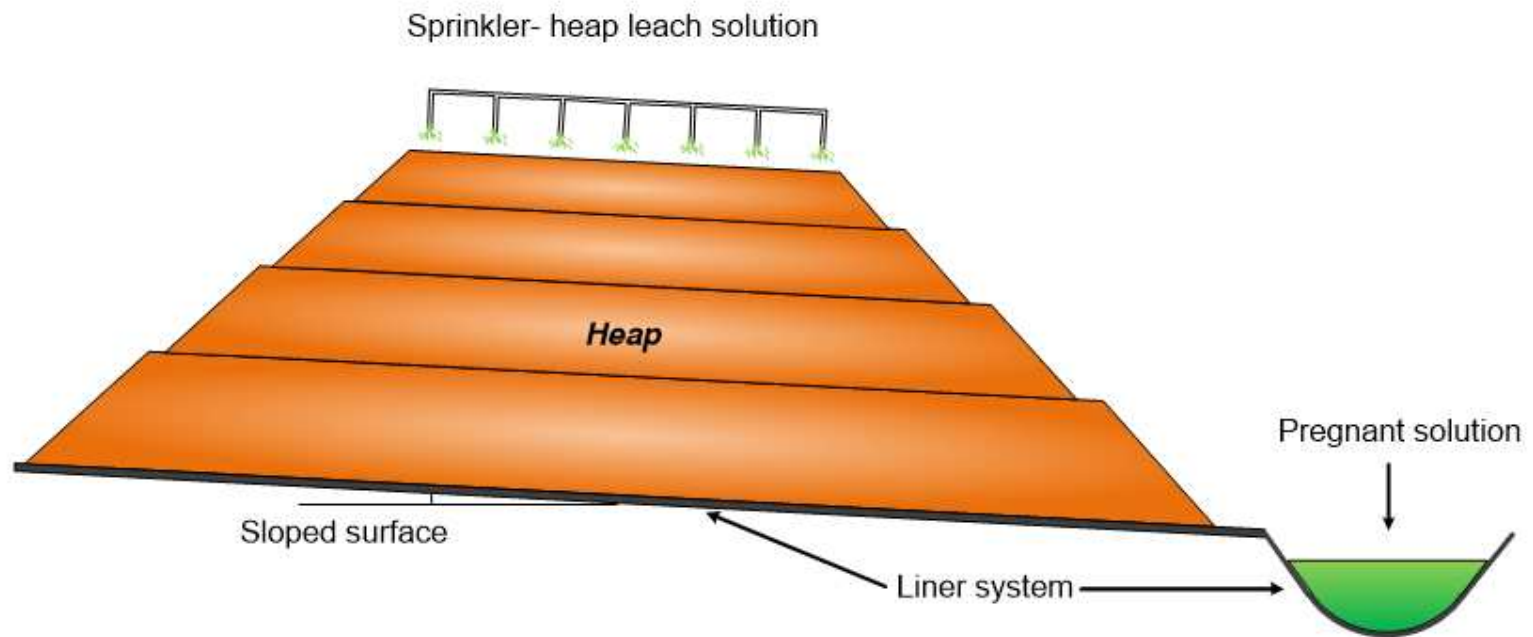


Fig. 1.1. Cross-sectional schematic of a heap leach facility.

## **CHAPTER 2: BACKGROUND**

This study primarily focused on development of an apparatus to evaluate internal shear strength behavior of GCLs for use in mining applications. A brief history of GCLs, types of GCLs, and field and laboratory shear strength testing of GCLs are provided in this section. Manufactured properties and test-conditions that affect the measured internal shear strength of GCLs are summarized to capture the state-of-art on GCL shear testing. Finally, a discussion on evaluation and interpretation of shear test data is also included. The focus in this study, and corresponding literature review, was on internal shear strength of needle-punched reinforced GCLs (NP-GCLs) evaluated in displacement-controlled direct shear tests at a constant displacement rate.

### **2.1 Geosynthetic Clay Liners**

#### *2.1.1 Brief History*

Environmental impacts attributed to leakage of landfill leachate into groundwater systems were mostly neglected before the 1970s due to lack of regulations. The Resource Conservation and Recovery Act (RCRA) legislated by congress in 1976 was the first comprehensive set of regulations related to management of waste disposal and containment. Waste containment systems (i.e., liners and covers) that included hydraulic barriers were introduced by RCRA to decrease contaminant migration into the environment.

In late 1980s and early 1990s GCLs were developed as an alternative hydraulic barrier to compacted clay liners commonly used in waste containment systems (US EPA 1987; US EPA 1991; Gilbert et al. 1996). As the GCL market grew during the 1990s, the U.S. Environmental Protection Agency (EPA) identified critical research needs related to the engineering properties and long-term performance of GCLs, which included hydraulic conductivity, bearing capacity, slope stability (shear strength), long-term reliability, and effects of



freeze and thaw cycling (US EPA 1997). Considerable research has been conducted since the U.S. EPA (1997) statement that has led to a broad range of standardized laboratory test methods to evaluate engineering properties of GCLs for design (e.g., ASTM D5889, D5887, D5890, D5891, D5993 and D6243).

During the 1990s and 2000s, hydraulic and mechanical properties (e.g., interface and internal shear strength) of GCLs were investigated by numerous researchers to enhance GCL design and expand applicability. Studies ranged from evaluations of hydraulic properties of GCLs permeated with non-standard liquids (e.g., Shackelford et al. 2000; Shackelford et al. 2010) to assessments of interface and internal shear strength of GCLs for a broad range of  $\sigma_n$  applications (e.g., Olsta and Swan 2001; Fox and Stark 2004). These research efforts have led to growth in the GCL market via application in diverse engineering projects. In 2014, 118-million  $m^2$  of GCL was sold world-wide with more than 30-million  $m^2$  sold in the U.S. for containment applications such non-hazardous solid waste, residential and commercial wastewater management, roadways, and other civil engineering construction projects. There is expectation that the GCL market will continue to grow such that the estimated value of this market in the U.S. will be nearly 500 million USD by 2022 (Research Grandview 2016).

### *2.1.2 Type of Geosynthetic Clay Liners*

Geosynthetic clay liners can be manufactured as unreinforced materials, which include no internal reinforcement passing through bentonite layer, or reinforced materials, which include stitch-bonded (SB) or needle-punched (NP) mechanical reinforcement within the bentonite layer. Schematics of SB-GCLs and NP-GCLs are shown in Fig. 2.1. Needle-punched GCLs typically have a non-woven (NW) or woven (W) geotextile (GT) as the cover GT and a NW or W GT as the carrier GT, whereas SB-GCLs can have NW-GTs or W-GTs as either carrier or cover GTs. In NP-GCLs, fibers from the NW-GT are punched-through the bentonite layer via needles and left entangled in the other NW or W GT to create structural reinforcement between the two

GTs and internal reinforcement within the bentonite clay layer (von Maubeuge and Heerten 1994). Geotextile fibers that are punched through the bentonite and entangled in the carrier GT can be thermally-treated to bond the reinforcement fibers to the carrier GT. This process is referred to as thermal-bonding, heat-bonding, or thermal-locking based on the GCL manufacturer. Stitch-bonded GCLs have parallel stitching across the cover and carrier GTs and these reinforcements can also be thermally-treated (Bouazza 2002).

## **2.2 Field-Scale Testing of Geosynthetic Clay Liners**

In 1994, the U.S. EPA supported construction of 14 field-scale GCL test sections on 3H:1V and 2H:1V slopes that simulated landfill final cover systems (Daniel et al 1998). A generalized cross-sectional schematic of a GCL test section is shown in Fig. 2.2. Final constructed test sections included nine on 2H:1V slopes that were approximately 9-m wide by 20-m long and five on 3H:1V slopes that were approximately 9-m-wide by 29-m long. All 3H:1V test sections were stable throughout the observation period. However, in the 2H:1V test sections, two interface failures occurred after initial construction (i.e., 20 and 50 d) and one internal failure occurred 495 d after construction.

The interface failures developed between the woven GT of the reinforced GCLs and textured geomembrane (GMX). These failures were attributed to bentonite hydration from the subgrade soil and subsequent bentonite extrusion through the woven GT into the interface between the GCL and GMX, which reduced interface friction and led to failure. Internal failure occurred due to unexpected bentonite hydration of an unreinforced, GMX-supported, GCL. Laboratory shear strength testing was conducted to assess interface and internal strength properties of relevant geosynthetic and earthen layers used in the test sections. Limit-equilibrium slope stability analyses conducted with laboratory measured shear strength parameters confirmed observations of the test section failures. This field study confirmed that laboratory testing combined with conventional slope stability analysis was a valid approach to

evaluate internal and interface stability of GCLs for cover design (Stark and Eid 1996; Daniel et al. 1998)

## **2.3 Laboratory-Scale Testing of Geosynthetic Clay Liners**

An extensive review on testing and applicability of GCL shear strength was recently completed by Fox and Stark (2015). Internal shear strength of GCLs most commonly is conducted via displacement-control tests at multiple  $\sigma_n$  to develop a failure envelope. These displacement-controlled tests are effective in capturing peak and large-displacement strength for internally-reinforced GCLs. Shear stress-controlled tests also can be performed via applying a constant shear force, constant stress rate, or incrementally increasing shear stress (Fox and Stark 2015).

### *2.3.1 Shear Strength Testing*

Schematics of three different laboratory apparatuses to measure the internal shear strength of GCLs are shown in Fig. 2.3. These three apparatuses include (i) traditional direct shear, (ii) ring shear, and (iii) inclined plane shear. Traditional direct shear tests (Fig. 2.3a) are the most common approach used to evaluate internal shear strength of GCLs (e.g. Gilbert 1996; Berard 1997; and Fox et al. 1997). This testing approach is based on conventional direct shear testing for soils in that a normal force is applied vertically on top of specimen, the upper and lower halves of the direct shear box are forced apart at a constant rate, and the shear force required to push or hold one half of the shear box in place is measured. The main difference between soil testing and GCL testing in a direct shear apparatus is that gripping and clamping systems are required to “lock” the GCL specimen to the upper and lower shear platens.

Ring shear testing of GCLs (Fig. 2.3b) has also been developed based on test methods for soil and is an effective test method to obtain very large-displacement (i.e., residual) internal shear strength since there is no limit on maximum displacement (e.g. Stark and Eid 1993, 1996;

Eid and Stark 1997; Eid et al. 1999). The third method to evaluate the internal shear strength of GCLs is an inclined plane shear device (Fig. 2.3c). This approach induces a constant ratio of normal and shear stress based on inclination of the plates and has primarily been used for force-controlled creep shear tests (e.g. Muller et al. 2008).

### 2.3.2 Analysis of Shear Behavior and Shear Strength

Post-testing analyses for internal shear strength experiments conducted on GCLs in a displacement-controlled direct shear apparatus include visual inspection of the GCL and data analysis. Visual inspection of the GCL includes measuring final specimen dimensions and bentonite water content, but also closely inspecting the GCL for possible tearing or local failures in the geosynthetics on surfaces in contact with the gripping plate and also at clamping locations. Bentonite water content often is measured at multiple locations to assess variability in water content and compute an average for the test specimen (Fox and stark 2004). The main shear data obtained from a given experiment include shear stress versus horizontal displacement relationship and vertical displacement versus horizontal displacement. Peak and large-displacement (residual) shear strength should be determined from each test conducted at a different  $\sigma_n$  to develop failure envelopes.

#### 2.3.2.1. Shear Stress versus Horizontal Displacement

A schematic of a shear stress versus horizontal displacement ( $\tau$ - $\delta_h$ ) relationship obtained from an internal shear strength test on a NP-reinforced GCL is shown in Fig. 2.4 (Fox and Stark 2004). At the start of the test, shear stress increases almost linearly with displacement and ultimately reaches a peak shear stress that is synonymous with peak shear strength ( $\tau_p$ ). After the peak stress is achieved, shear stress decreases due to fiber rupture and/or pullout in NP-GCLs until a large-displacement ( $\tau_{ld}$ ) or residual shear stress ( $\tau_r$ ), which can also be taken as

measurements of large-displacement or residual shear strength. The residual shear strength represents failure of all reinforcing elements and shear resistance is only due to frictional resistance within the bentonite clay and at the interface between bentonite and GTs of the GCL. The magnitude of  $\tau_{ld}$  may not be a true measure of  $\tau_r$  depending on the amount of horizontal displacement, but often  $\tau_{ld}$  and  $\tau_r$  are assumed comparable and representative of a constant shear stress with continued horizontal displacement following complete reinforcement fiber pullout and/or rupture.

### 2.3.2.2. Failure Envelopes for Needle-Punched GCLs

A schematic of potential failure envelopes that can be developed for NP-reinforced GCLs is shown in Fig. 2.5. Fox and Stark (2004) report that failure envelopes for internal peak shear strength of GCLs are generally nonlinear and a single linear Mohr-Coulomb failure envelope may not be adequate to characterize shear strength parameters. Possible failure envelopes for internal shear strength of NP-GCLs include linear, multi-linear, or nonlinear relationships that may or may not have an intercept.

Linear or multi-linear failure envelopes can be defined via traditional Mohr-Coulomb relationships:

$$\tau = c + \sigma_n \cdot \tan \phi \quad (2)$$

where  $\tau$  = shear strength,  $c$  = cohesion intercept,  $\sigma_n$  = normal stress, and  $\phi$  = internal angle of friction. This formula can be used to determine strength parameters for peak and large-displacement internal shear strengths, and the formula can also be applied to different ranges of  $\sigma_n$  to determine multi-linear failure envelopes (Fox and Stark 2004).

The following nonlinear model from Duncan and Chang (1970) was used by Gilbert et al. (1996) to assess peak interface and internal shear strength of a NP-GCL:

$$\tau_p = \sigma_n \tan \left[ \phi_o + \Delta\phi \log \left( \frac{\sigma_n}{P_a} \right) \right] \quad (3)$$

where  $\tau_p$  = peak shear strength,  $\phi_o$  and  $\Delta\phi$  are regression constants representing of nonlinear frictional dependent strength, and  $P_a$  = atmospheric pressure. Giroud et al. (1993) proposed the following p-order hyperbola with non-orthogonal asymptotes as a nonlinear envelope:

$$\tau_p = a_\infty + \sigma_n \tan \delta_\infty - \frac{a_\infty - a_o}{\left( 1 + \frac{\sigma_n}{\sigma_o} \right)^p} \quad (4)$$

where  $a_\infty$ ,  $\delta_\infty$ ,  $a_o$ , and  $\sigma_o$  = constants. Fox et al. (1998) and Theis et al. (2002) used this nonlinear model for internal shear strength of GCLs; however, a considerable amount of data points are needed to achieve an appropriate fit with the nonlinear model in Eq. 4.

## 2.4 Factors Affecting Shear Behavior and Strength of GCLs

A summary of relevant studies on the internal shear strength of NP-GCLs that employed traditional direct shear apparatuses is in Table 2.1. Factors affecting the internal shear strength of reinforced GCLs can be classified into two categories: (i) manufactured properties of GCLs and (ii) shear testing conditions and procedures. Manufactured properties of GCLs that affect internal shear strength of GCLs primarily deal with the type and strength of reinforcement fibers as well as the mechanism via which reinforcement fibers are attached to the carrier GT. Shear testing conditions and procedures include the shearing  $\sigma_n$ , hydration and consolidation procedure, hydration liquid, gripping and clamping system, displacement rate, machine direction, and testing temperature.

### 2.4.1 Manufactured Properties of GCLs

Geosynthetic clay liners include a broad range of physical properties based on innovations from different GCL manufacturers and targeted engineering application. Unreinforced GCLs have low shear strength analogous to hydrated bentonite, and are constrained to applications with negligible ground slope. Stark et al. (1998) reported a failure that occurred along the hydrated bentonite in landfill liner where a geomembrane-backed GCL was installed along the bottom and side slopes of the landfill. On the other hand, reinforced GCLs are more applicable for geotechnical engineering applications as the SB or NP reinforcements enhance the internal shear strength of the GCL.

#### 2.4.1.1 Type of Reinforcement

Fox et al. (1998) performed direct shear tests on unreinforced GCLs as well as SB- and NP-reinforced GCLs to compare internal peak and large-displacement shear strength (Table 2.1 and 2.2). Failure envelopes of four GCL products tested as a part of their study are shown in Fig 2.6. All specimens were hydrated under 1 kPa for 2 d and then under the target  $\sigma_n$  (7 to 279 kPa) for an additional 2 d prior to shearing at a constant displacement-rate of 0.1 mm/min. Failure envelopes for NP- and SB-GCLs have higher peak shear strength than unreinforced GCLs (Fig. 2.6); however, large-displacement shear strength of all GCLs were comparable due to failure occurring within the bentonite at the boundary of a GT layer at large-displacement for both reinforced and unreinforced GCLs. An increase in peak strength with increasing target  $\sigma_n$  was observed for SB-GCLs at  $\sigma_n < 72$  kPa; however; as  $\sigma_n$  increased above 72 kPa, peak shear strength was approximately constant at 91 kPa (Fig. 2.6). Constant shear strength at higher  $\sigma_n$  for the SB-GCL was due to localized failure at the connections between stitches and the GT rather than failure within the stitches. In contrast, NP-GCLs exhibited an increase in peak shear strength with increasing  $\sigma_n$  that is analogous to frictional behavior of soils. Also, an increase in

peel strength for the NP-GCLs yielded an increase in peak shear strength. The frictional behavior of NP-GCLs relative to SB-GCLs renders NP reinforcements as a more attractive design alternative in reinforced GCLs relative to SB, particularly for high target  $\sigma_n$  applications.

#### 2.4.1.2 Reinforcement Fibers and GCL Peel Strength

Peel strength of NP-reinforced GCLs is an index of the relative strength and density of interlocking fibers (Fox and Stark 2004) that can be assessed using standardized testing techniques (ASTM D6496, ASTM 2011). Several studies have investigated relationships between peel strength and internal shear strength of GCLs (Berard 1997; Richardson 1997; Fox et al. 1998; Olsta and Crosson 1999; von Maubeuge and Lucas 2002; Zornberg et al. 2005, Athanassopoulos and Yuan 2011). Berard (1997) observed an increase in the internal friction angle of NP-GCLs with increase in peel strength for dry, partially hydrated, and fully-hydrated specimens. Richardson (1997) reported that peel strength measured on dry GCLs can be used an index of internal shear strength of hydrated GCLs and also that an increase in peel strength corresponded to an increase in internal shear strength.

Experimental results of peak shear strength versus  $\sigma_n$  from three studies (Fox et al. 1998; Zornberg et al. 2005; Athanassopoulos and Yuan 2011) that incorporated NP-GCLs with a range of peel strengths are shown in Fig 2.7. Data compiled from Fox et al. (1998) indicate that GCLs with higher peel strength have higher peak shear strength for a range of  $\sigma_n$  from 38 to 280 kPa. Athanassopoulos and Yuan (2011) conducted a series of direct shear tests on NP-GCLs with varying peel strength (Fig. 2.7) and developed a correlation whereby peak shear strength increased as a function of average peel strength for  $\sigma_n$  ranging from 240 to 720 kPa. However, Zornberg et al. (2005) concluded from a large database on GCL internal shear that peel strength variability had a minor impact on internal peak shear strength of NP-GCLs. Zornberg et al. (2005) attributed the absence of a trend between peel strength and peak shear



strength to different mechanisms of fiber mobilization and variations in shear strength testing. However, a universal finding from all studies was that there is no relationship between peel strength of NP-GCLs and large-displacement or residual shear strength. This behavior is attributed to complete pullout or rupture of all reinforcement fibers such that large-displacement or residual shear strength only are a function of the internal friction angle of bentonite clay and possible interface interactions between the clay and GTs of a GCL.

#### 2.4.1.3 Thermal-Bonding of Reinforcement Fibers

Needle-punched GCLs can be thermally treated to decrease fiber pullout during shear and potentially increase peak shear strength. The database of GCL shear strength compiled in Zornberg et al. (2005) contained thermally-bonded GCLs that allowed comparison to non-thermally-bonded GCLs. Non-thermally-bonded GCLs had a slightly higher peak shear strength compared to thermally-bonded GCLs for low  $\sigma_n$  ( $\approx 50$  kPa); however, this trend reversed for  $\sigma_n = 300$  kPa. Zornberg et al. (2005) concluded that thermal bonding enhances peak shear strength of GCL under higher  $\sigma_n$  and reduced horizontal displacements to peak strength.

### 2.4.2 *Shear Testing Conditions of Geosynthetic Clay Liners*

#### 2.4.2.1 Hydration and Consolidation

The bentonite layer in GCLs can absorb water from underlying soils or overlying waste to create a low hydraulic conductivity barrier (Daniel et al. 1993). The internal peak and large-displacement shear strengths of GCLs are dependent on bentonite hydration and chemistry of the hydration liquid. In general, GCL internal shear strength for a given normal stress decreases with increasing bentonite hydration and is lowest when bentonite is fully hydrated. Thus, hydration procedures adopted in laboratory test methods should simulate anticipated field conditions pertaining to normal stress and liquid chemistry, and also tend towards full-hydrated

GCLs to assess the anticipated critical hydration conditions. Three factors should be considered for GCL hydration: (i) hydration time ( $t_h$ ), (ii) hydration normal stress ( $\sigma_{n-h}$ ), and (iii) hydration solution (Fox and Stark 2004).

There are several approaches for hydrating GCL specimens, including hydrating under the target  $\sigma_n$  for shear testing or hydrating under a lower  $\sigma_n$  (i.e.,  $\sigma_{n-h}$ ) followed by consolidation to the target  $\sigma_n$  prior to shear testing. Gilbert et al. (1997) introduced a hydration factor as an indicator of hydration completeness. The hydration factor (HF) is defined as:

$$HF = \left| \frac{h_t - h_{t-12hr}}{h_t} \right| \quad (1)$$

where  $h_t$  = GCL height at time  $t$  and  $h_{t-12hr}$  = GCL height 12 h before time  $t$ . If  $HF < 5\%$ , Gilbert et al. (1997) recommended that GCL hydration can be assumed complete. Gilbert et al. (1997) reported effective GCL hydration ranging from  $t_h = 2.6$  to 24.7 d for  $\sigma_{n-h}$  ranging from 69 to 3.5 kPa. The increase in  $t_h$  with a decrease in  $\sigma_{n-h}$  was due to a greater ability of bentonite clay to attract water and swell at lower effective stress. Gilbert et al. (1997) reported that  $t_h \approx 20$  d for GCL shear testing may be excessively long for practical applications and would affect marketability of GCLs. Thus, shorter hydration times should be considered in practice.

Fox et al. (1998) recommended a two-stage accelerated hydration procedure, whereby a GCL is first hydrated outside the shear device under  $\sigma_{n-h} = 1$  to 2 kPa for 48 h. Following this first stage, the GCL is then placed into the shear device,  $\sigma_n$  is increased to the target  $\sigma_n$  for shear testing, and the GCL is allowed to hydrate for an additional 2 d before shearing. McCartney et al. (2009) evaluated hydration effects on GCLs and reported that internal peak shear strength at a given  $\sigma_n$  ranging from 2.4 to 100 kPa decreased with increasing  $t_h$  to 48 h, and was constant for longer hydration times. These studies suggest that a minimum hydration time of 2 d is likely reasonable to measure the internal shear strength of GCLs.

Chemistry of the hydration liquid affects water-clay interactions in the diffuse double layer of bentonite clay that can increase or decrease swell of the clay layer. For example, the internal friction angle of montmorillonite clay was reported to more than double when the major cation on the exchange complex of the clay mineral was changed from sodium ( $\text{Na}^+$ ) to calcium ( $\text{Ca}^{2+}$ ) (Mesri and Olson 1970). Koerner (1998) conducted direct shear tests on four different GCLs hydrated in de-ionized water, tap water, moderated-strength landfill leachate, high-strength landfill leachate, and diesel fuel. An increase in shear strength of the GCLs was observed due to cation exchange and reduction in bentonite swell. De-ionized water consistently yielded the smallest peak shear strengths among the different GCLs and was considered the most conservative hydration liquid for shear strength testing (Koerner 1998).

Specimens hydrated at  $\sigma_{n-h} < \sigma_n$  must be consolidated prior to shearing. Few studies have investigated the influence of consolidation time ( $t_c$ ) and procedure on peak and large-displacement internal shear strength of reinforced GCLs. McCartney (2009) conducted a study on the effect of consolidation on peak internal shear strength of a W/NW NP-GCL, and peak shear stress versus normal stress results from this study are shown in Fig 2.8. Two different hydration and consolidation procedures were used: (i) specimens were hydrated for  $t_h = 24$  h and sheared immediately after hydration (i.e., no time allowed for consolidation) and (ii) specimens were hydrated for  $t_h = 60$  h and then allowed to consolidate under the target shearing  $\sigma_n$  for 24 h. All specimens were hydrated under  $\sigma_{n-h} = 7$  kPa and sheared at a displacement rate of 1 mm/min. McCartney et al. (2009) observed similar peak shear strength for both sets of tests and reported that time allowed for the GCL to consolidate before shearing did not have a considerable impact on measured peak shear strength. However, regardless of time allowed for GCL consolidation prior to shearing, the application of  $\sigma_n$  (e.g., any  $\sigma_n > \sigma_{n-h}$ ) should be applied incrementally to prevent bentonite extrusion out of the GCL, particularly for GCLs that included a woven GT. Thus, stepwise loading of GCL specimens should be

conducted to reach the target  $\sigma_n$  for shear testing and subsequently the GCL specimen should be allowed to equilibrate under the final target  $\sigma_n$  in the shear box for at least 24 h before shearing (Fox and Stark 2004).

#### 2.4.2.2 Normal Stress

The normal stress under which shear testing is conducted ( $\sigma_n$ ) is dependent on application of the GCL, ranging from low  $\sigma_n$  for cover systems to higher  $\sigma_n$  for liner systems. Peak shear strength of NP-GCLs discussed previously in Figs. 2.6 to 2.8 indicates that GCLs exhibit frictional behavior whereby an increase in  $\sigma_n$  corresponds to an increase in shear strength. According to ASTM D6243 (2013) at least three  $\sigma_n$  are needed to develop a shear strength envelope for GCLs; however, the  $\sigma_n$  range should be selected carefully due to nonlinearity of shear strength envelopes for GCLs (Fox and Stark 2004).

#### 2.4.2.3 Geotextile Gripping and Clamping

Critical aspects of GCL shear testing include the gripping surface and clamping system of the shear platens that secure the GTs of a GCL specimen to the upper and lower shear platens. These components are critical such that the shear force developed along the interface between the shear platens and GCL specimen are transferred across the interfaces and uniformly into the internal region of the GCL. The shear platen gripping surfaces must maintain effective contact with both GTs of a GCL throughout the experiment and allow free movement of water into and out of the specimen.

ASTM D6243 (2015) recommends that gripping surfaces be constructed of textured steel composed of rasps, truss plates, nail boards, or machined spikes that are 1 to 2 mm tall and mounted on a rigid surface. Shear stress versus horizontal displacement relationships for direct shear tests conducted by Allen and Fox (2007) on a W/NW NP-GCL (peel strength = 458

N/m) that included three different gripping surfaces are shown in Fig 2.9. Detailed descriptions of each gripping surface are in Table 2.3. Stress-displacement relationships for tests at  $\sigma_n = 9.6$  kPa exhibit jagged behavior that is representative of slippage between the GTs of the GCL and gripping surfaces. However, as  $\sigma_n$  was increased, stress-displacement behavior was smoother for all three gripping surfaces. Potential for slippage between the gripping surfaces and GTs of the GCL indicate that the gripping surface was not capable of effectively transferring shear forces to interlocking fibers of the GCL. Visual inspections following these experiments confirmed interpretations made based of stress-displacement relationships. Allen and Fox (2007) concluded that pyramid-tooth gripping plates were the most effective gripping method among the surfaces evaluated to internally shear GCL specimens.

#### 2.4.2.4 Shear Displacement Rate

The internal shear strength of NP-GCLs is dependent on the rate of shear displacement. Stark and Eid (1996) and Eid et al. (1999) performed torsional ring shear tests on a thermally-locked NP-GCL at displacement rates ranging from 0.015 to 36.5 mm/min. Peak shear strength for experiments conducted at  $\sigma_n = 17$  to 400 kPa are shown in Fig 2.10 as a function of displacement rate. In general, peak shear strength increased with increasing displacement rate from 0.01 to 1.0 mm/min for experiments conducted at  $\sigma_n \leq 100$  kPa. Experiments conducted at higher  $\sigma_n$  (200 and 400 kPa) exhibited negligible effects of displacement rate on peak shear strength for displacement rates  $\leq 1.0$  mm/min. The complicated behavior shown in Fig. 2.10 was attributed to three mechanisms: (i) rapid pullout and tearing of reinforcement fibers, (ii) positive excess pore water pressure, and (iii) undrained frictional resistance of hydrated bentonite. ASTM D6243 (2013) and Fox and Stark (2015) recommended that hydrated reinforced GCLs should be tested at a displacement rate of 0.1 mm/min to obtain drained internal shear strength.

#### 2.4.2.5 Temperature

Biological and chemical reactions in waste containment and heap leach facilities (e.g., aerobic and anaerobic biodegradation, aluminum production waste reactions, etc.) can lead to elevated temperatures within the waste mass and also on barrier systems (Smith 2008; Martin et al. 2013). Studies on landfill temperatures report internal waste mass temperatures  $> 60^{\circ}\text{C}$  depending on waste type, waste density, climate, and operational procedure (Rowe 2005; Hanson et al. 2010; Bouazza et al. 2011). Elevated temperatures of 45 and  $75^{\circ}\text{C}$  reported in copper and nickel heap leach facilities (Smith 2008). There is a need to understand the engineering properties and behavior of GCLs used in barrier systems that can be subjected to elevated temperatures. However, currently there have been no studies conducted to evaluate internal shear strength of GCLs via displacement-controlled experiments at elevated temperatures (Fox and Stark 2015).

Table 2.1. Direct shear tests on internal shear strength of needle-punched reinforced geosynthetic clay liners.

Reference <sup>a</sup>	GCL Type	Specimen Size: W x L (mm)	Max. Shear Displacement (mm)	Peel Strength (N/m)	Hydration Conditions	Shearing Normal Stress, $\sigma_n$ (kPa)	Shear Rate (mm/min)	Peak Shear Strength		Large-Displacement Shear Strength	
								$c_p$ (kPa)	$\phi_p$ (°)	$c_{ld}$ (kPa)	$\phi_{ld}$ (°)
Byrne (1994)	NP (W/NW)	-	43-51	NR	Hydrated; time NR	96-479	-	19.2	16	5.8	4.6
Fuller (1995)	NP (W/NW)	-	98-102	NR	$\sigma_h = \sigma_n$ for 5 d	9.6-34.5	0.1	23	10.5	8.6	6
Garcin et al. (1995)	NP (W/NW)	-	45	NR	Unconfined hydration, 1 wk	15-150	0.5	74	0	-	-
Gilbert et al. (1996) <sup>b</sup>	NP (W/NW)	NR	36-43	NR	$\sigma_h = \sigma_n$ for 2.6-24.7 d	3.5-23	0.059-0.072	0	$\phi_o = 18^\circ$ , $\Delta\phi_o = -23^\circ$	0	$\phi_o = 9.8^\circ$ , $\Delta\phi_o = -16^\circ$
			NR	NR		23-69		0	$\phi_o = 30^\circ$ , $\Delta\phi_o = -4.7^\circ$	0	
Berard (1997)	NP (W/NW)	-	58-73	NR	$\sigma_h = \sigma_n$ 2 wk	25-100	0.1	10.5	134	-	-
Feki et al. (1997)	NP	-	40-45	NR	Dry	25-100	1	175	18	0	29
Richardson (1997)	NP	NR	NR	NR	NR	0-1200	1	40.8	21.4	13.5	6.2
Siebken et al. (1997)	Heat-bonded NP (W/NW)	300 x 300	50	NR	$\sigma_h = \sigma_n$ for 1 d	34-670	1	47	23	0.9	11

Note:  $ld$  = displacement;  $W$  = woven;  $NW$  = non-woven;  $NP$  = needle-punched;  $\sigma_h$  = hydration normal stress;  $\sigma_n$  = shearing normal stress;  $c_p$  = peak shear strength cohesion intercept;  $\phi_p$  = peak shear strength friction angle;  $c_{ld}$  = large-displacement shear strength cohesion intercept;  $\phi_{ld}$  = large-displacement shear strength friction angle; NR = not reported.

<sup>a</sup> Eid et al. (1999) conducted ring shear tests, direct shear testing was conducted for all other referenced studies

<sup>b</sup> Shear strength parameters for Gilbert et al. (1996) pertain to the nonlinear failure envelope in Eq. 3.

Table 2.1. Direct shear tests on internal shear strength of needle-punched reinforced geosynthetic clay liners (continued).

Reference <sup>a</sup>	GCL Type	Specimen Size: W x L (mm)	Max. Shear Displacement (mm)	Peel Strength (N/m)	Hydration Conditions	Shearing Normal Stress, $\sigma_n$ (kPa)	Shear Rate (mm/min)	Peak Shear Strength		Large-Displacement Shear Strength	
								$c_p$ (kPa)	$\phi_p$ (°)	$c_{ld}$ (kPa)	$\phi_{ld}$ (°)
Fox et al. (1998)	NP (W/NW)	305 x 1067	180-200	1600	$\sigma_h = 1$ kPa for 2 d, then $\sigma_h = \sigma_n$ for 2 d	6.9-279	0.1	98.2	32.6	1	4.7
	NP (W/NW)			850		6.9-141		42.3	41.9	1	4.7
Eid et al. (1999)	Heat-bonded NP (W/NW)	Ring Shear	87-98	NR	$\sigma_h = 17$ kPa for 2 wk	17-400	0.015	26.5	6.7	4.6	5.8
Olstad and Swan (2001)	NP (W/NW)	300 x 300; and 150 x 150	35-50	NR	$\sigma_h = \sigma_n$ for 2 d	350-1050	1	100	12	13	6
				NR		1050-2800					
Allen & Fox (2007)	NP (W/NW)	305 x 305	80	458	$\sigma_h = 9.6$ kPa for 1 d, then $\sigma_h = \sigma_n$ for 12 h	9.6-478.8	0.1	NR	NR	NR	NR
Athanasopoulos & Yuan (2011)	NP (W/NW)	300 x 300	75	44	$\sigma_h = 10$ kPa for 1 d, then $\sigma_h = \sigma_n$ for 1 d	239.5-718.4	1	10	9	NR	NR
				740				92	16	NR	NR
				1086				92	18	NR	NR
				1598				128	21	NR	NR
				1909				104	25	NR	NR
				2666				135	27	NR	NR
Fox & Ross (2011)	NP (NW/NW)	305 x 1067	180-200	2170	$\sigma_h = 1$ kPa for 2 d, then $\sigma_h = \sigma_n$ for 2 d	71.9-692	0.1	83.7	23.7	1.3	4.8
						692-2071		261	9.9		

Note:  $ld$  = displacement;  $W$  = woven;  $NW$  = non-woven;  $NP$  = needle-punched;  $\sigma_h$  = hydration normal stress;  $\sigma_n$  = shearing normal stress;  $c_p$  = peak shear strength cohesion intercept;  $\phi_p$  = peak shear strength friction angle;  $c_{ld}$  = large-displacement shear strength cohesion intercept;  $\phi_{ld}$  = large-displacement shear strength friction angle; NR = not reported.

<sup>a</sup> Eid et al. (1999) conducted ring shear tests, direct shear testing was conducted for all other referenced studies



Table 2.2. Direct shear testing summary from Fox et al. (1998).

GCL	Peel Strength (N/m)	Normal Stress (kPa)	Peak Shear Stress (kPa)	Horizontal Displacement to Peak (mm)	Residual Shear Strength (kPa)	Average Final Water Content (%)
GCL-1	-	6.9	3.6	2.4	1.7	273
GCL-1	-	24.0	8.5	1.5	3.8	194
GCL-1	-	37.8	12.0	1.5	5.0	189
GCL-1	-	72.2	18.3	1.5	7.3	148
GCL-1	-	141	28.7	1.4	13.3	149
GCL-2	-	279	52.7	1.6	22.2	105
GCL-2	-	24.0	73.5	63.1	4.7	188
GCL-2	-	37.8	68.6	53.0	6.2	163
GCL-2	-	72.2	86.3	46.5	9.8	135
GCL-2	-	72.2	92.5	51.0	9.3	140
GCL-2	-	141	83.2	39.7	15.6	115
GCL-2	-	279	91.4	44.6	26.6	81
GCL-3	1600	37.8	122.7	25.8	5.0	198
GCL-3	1800	72.2	160.3	21.5	9.0	158
GCL-3	1500	141	184.8	22.9	13.8	138
GCL-3	1600	279	276.8	23.2	22.0	101
GCL-3	850	17.1	62.4	23.5	3.8	228
GCL-3	850	37.8	75.8	16.5	5.6	191
GCL-3	850	72.2	114.5	16.9	9.3	137
GCL-3	850	141	169.3	20.4	-	121

Note: GCL-1 = Claymax 200RW (unreinforced GCL); GCL-2 = Claymax 600SP (SB GCL); GCL-3 = Bentomat ST (NP GCL)

Table 2.3. Description of shear platen gripping surfaces used in Allen and Fox (2007) to transfer shear force from shear platen onto the surface of the GCL during shear testing.

Gripping Surface	Description
Conventional	Truss plate with 1 to 2-mm-tall sharpened teeth attached to 7-mm-thick plywood and secured to 20-mm-thick plywood for shear platen
GRI-GCL4	Truss plate with 1.5-mm-tall flat teeth screwed to a 25-mm-thick PVC plate
Pyramid	Pyramid teeth machined into a 12.5-mm-thick stainless steel plate. Teeth were 2.3-mm tall for $\sigma_n < 50$ kPa and 1-mm tall for $\sigma_n > 450$ kPa

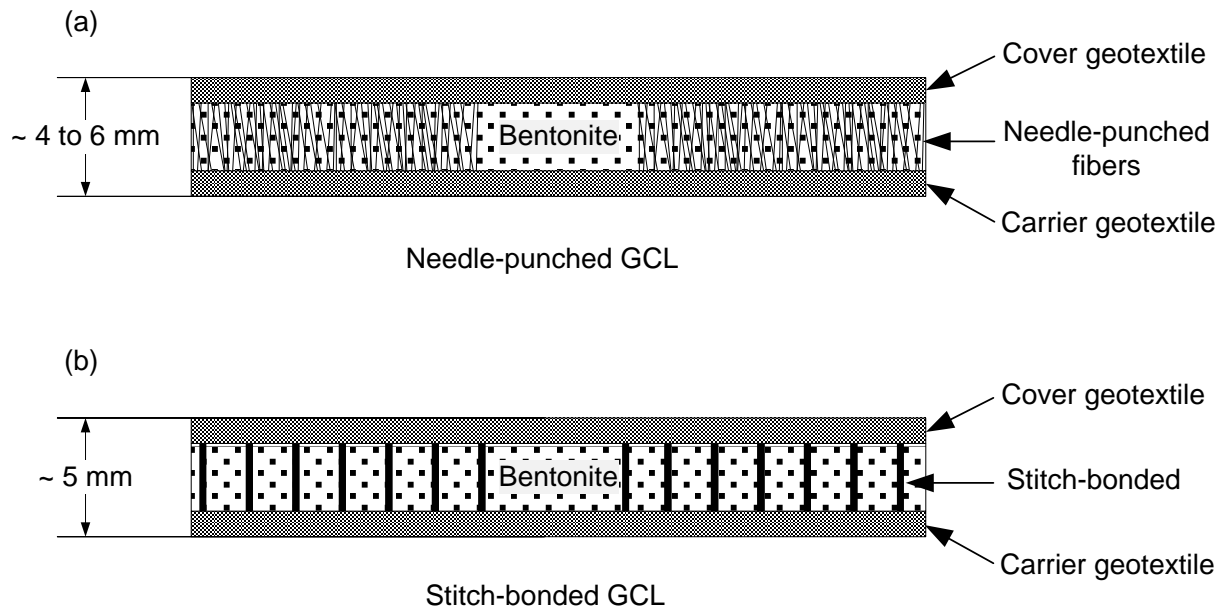


Fig. 2.1. Schematics of dry (a) needle-punched and (b) stitch-bonded internally-reinforced geosynthetic clay liners

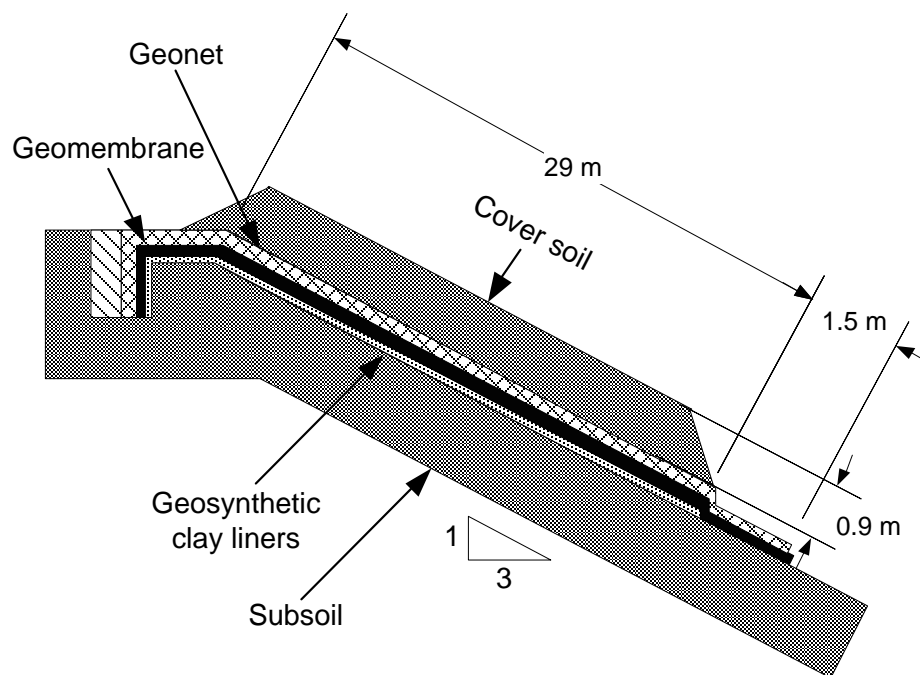


Fig. 2.2. Cross-section of an 3H:1V test plot constructed to evaluate interface/internal slope stability of cover systems employing a geosynthetic clay liner (Daniel et al. 1998).

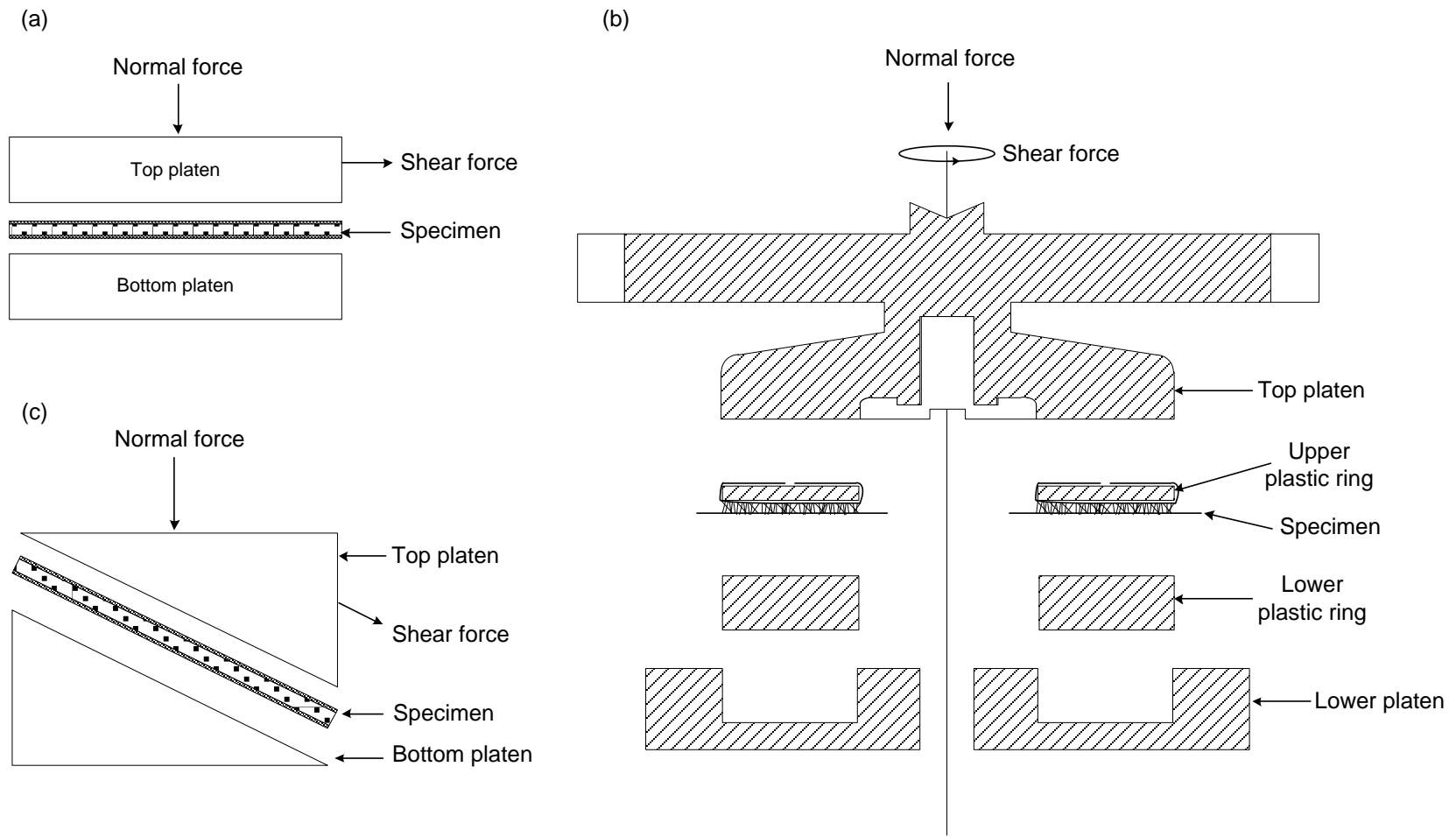


Fig. 2.3. Schematics of shear testing apparatuses: (a) direct shear, (b) ring shear, and (c) inclined plane shear (Not to scale).

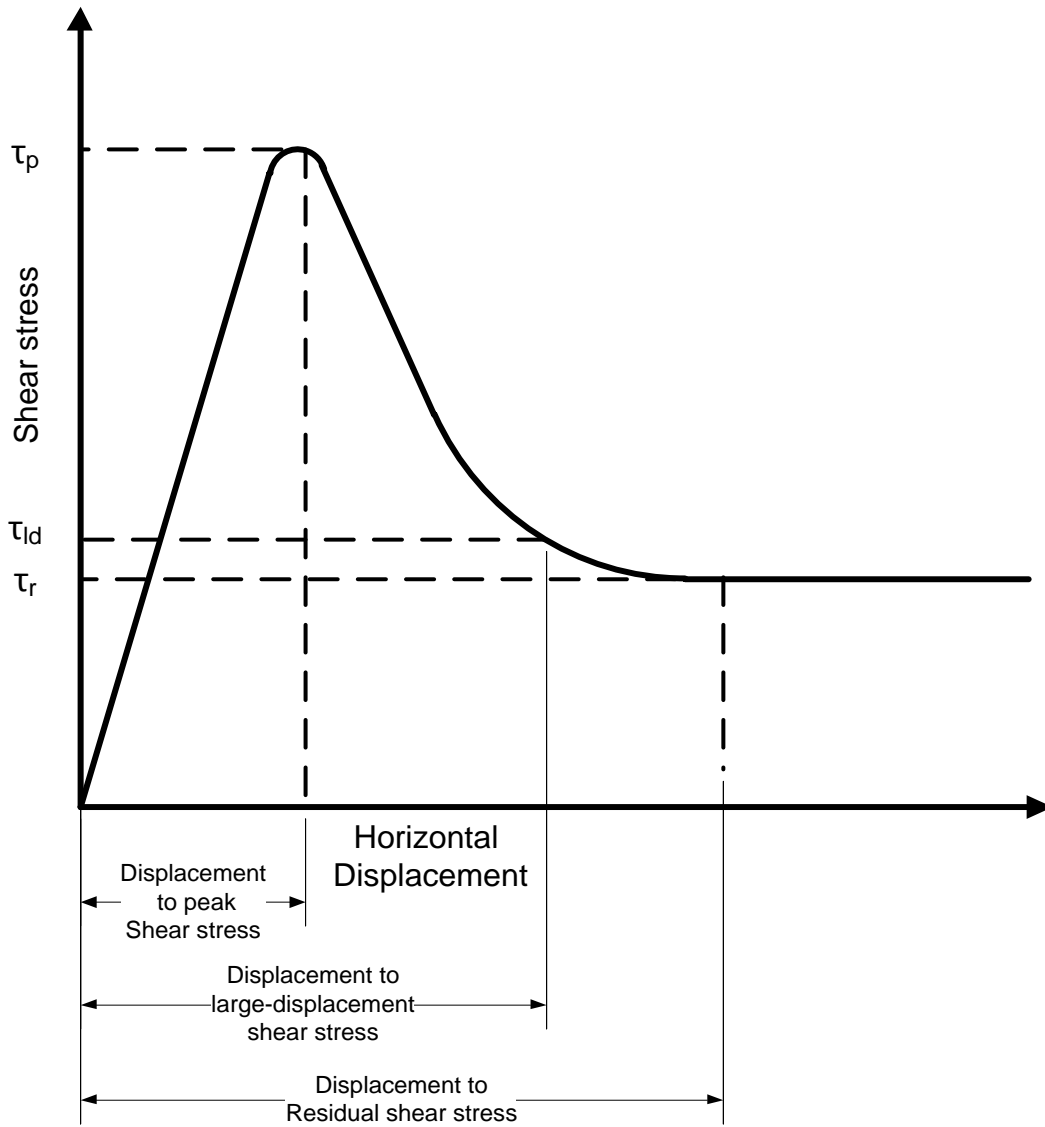
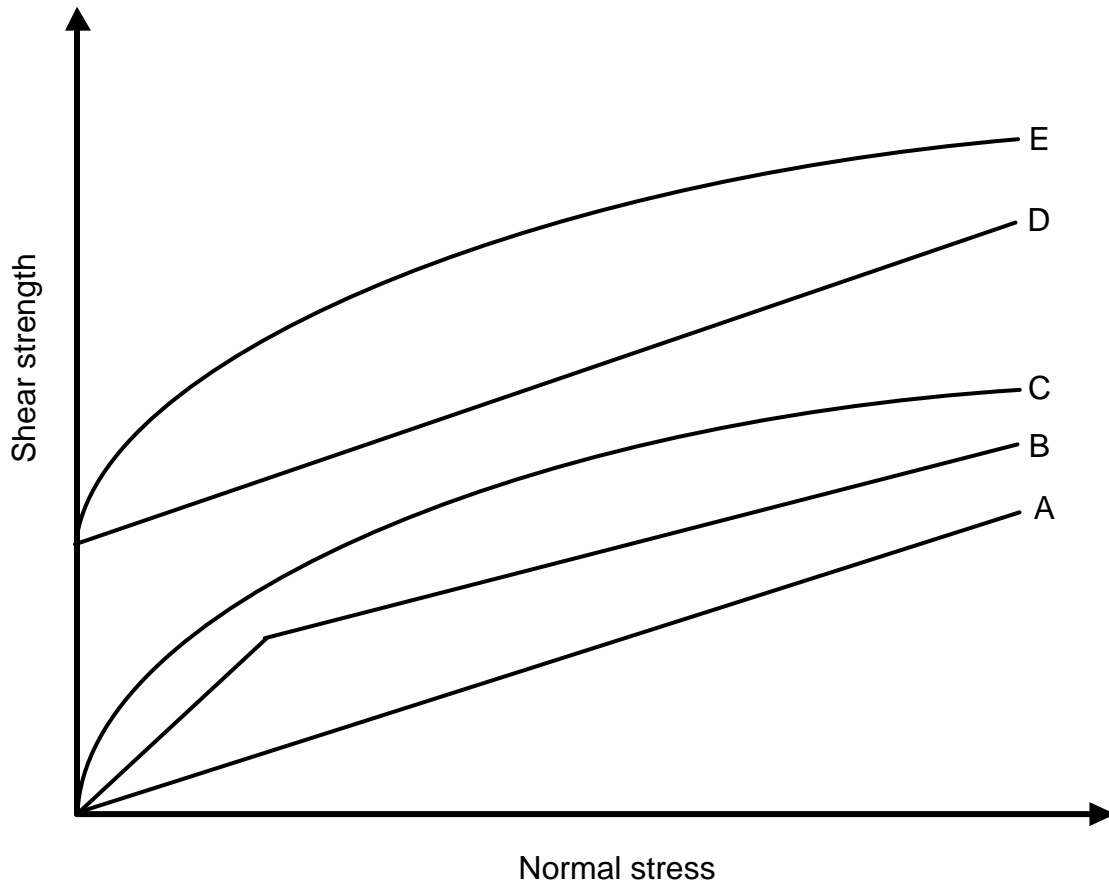


Fig. 2.4. Typical shear stress versus horizontal displacement relationship for internal shear strength testing of reinforced geosynthetic clay liners.



- |   |
|---|
| <p>A – Linear envelope passing zero intercept</p> <p>B – Multi-linear envelope</p> <p>C – Non-linear passing zero intercept</p> <p>D – Linear envelope with non-zero intercept</p> <p>E – Non-Linear envelope with non-zero intercept</p> |
|---|

Fig. 2.5. Example of typical failure envelopes to define shear strength parameters (Fox and Stark 2004).

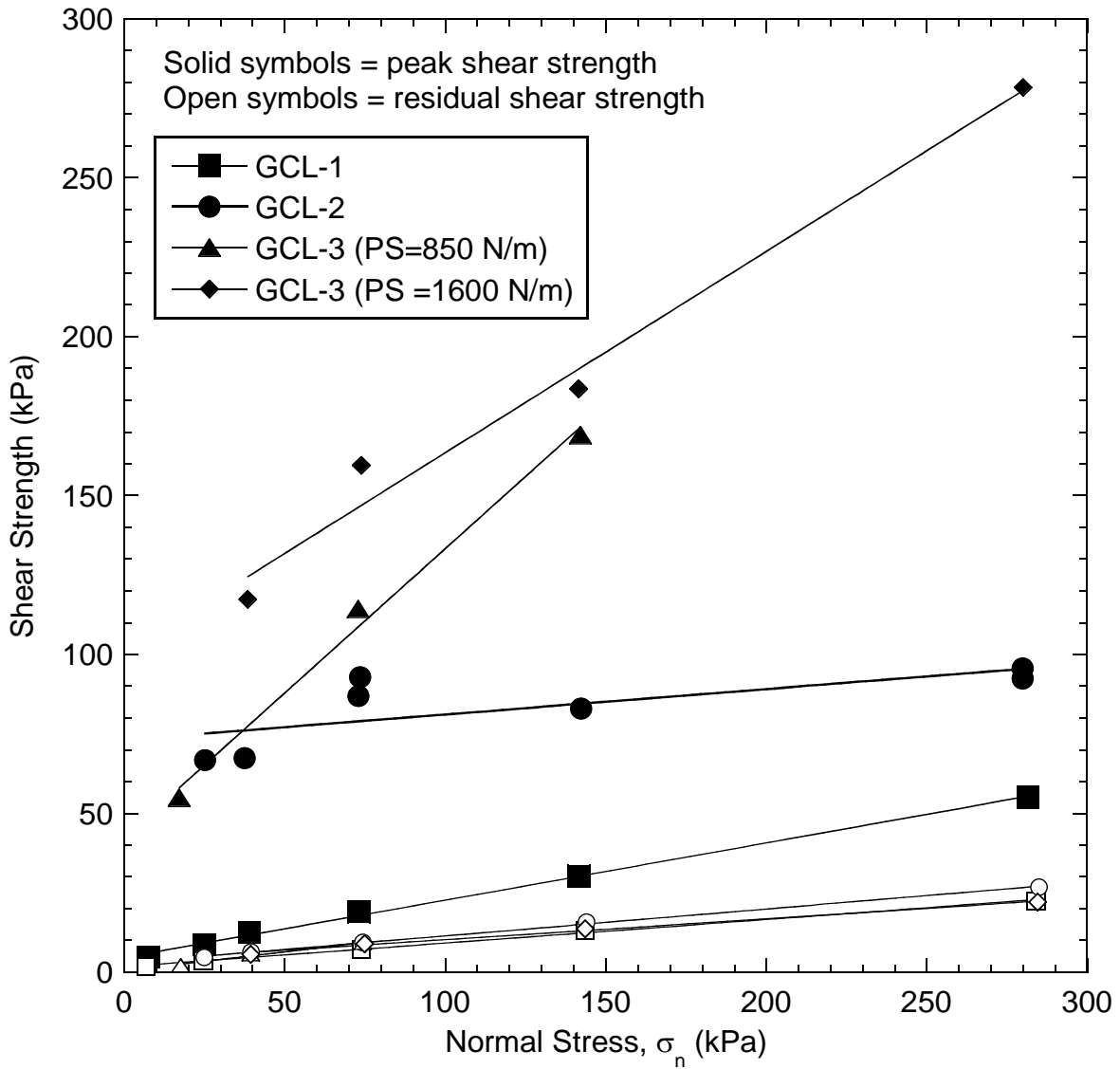


Fig. 2.6. Failure envelopes for peak and residual shear strength from Fox et al. (1998). Note: GCL-1 = unreinforced GCL, GCL-2 = stitch-bonded GCL, and GCL-3 = needle-punched GCL.



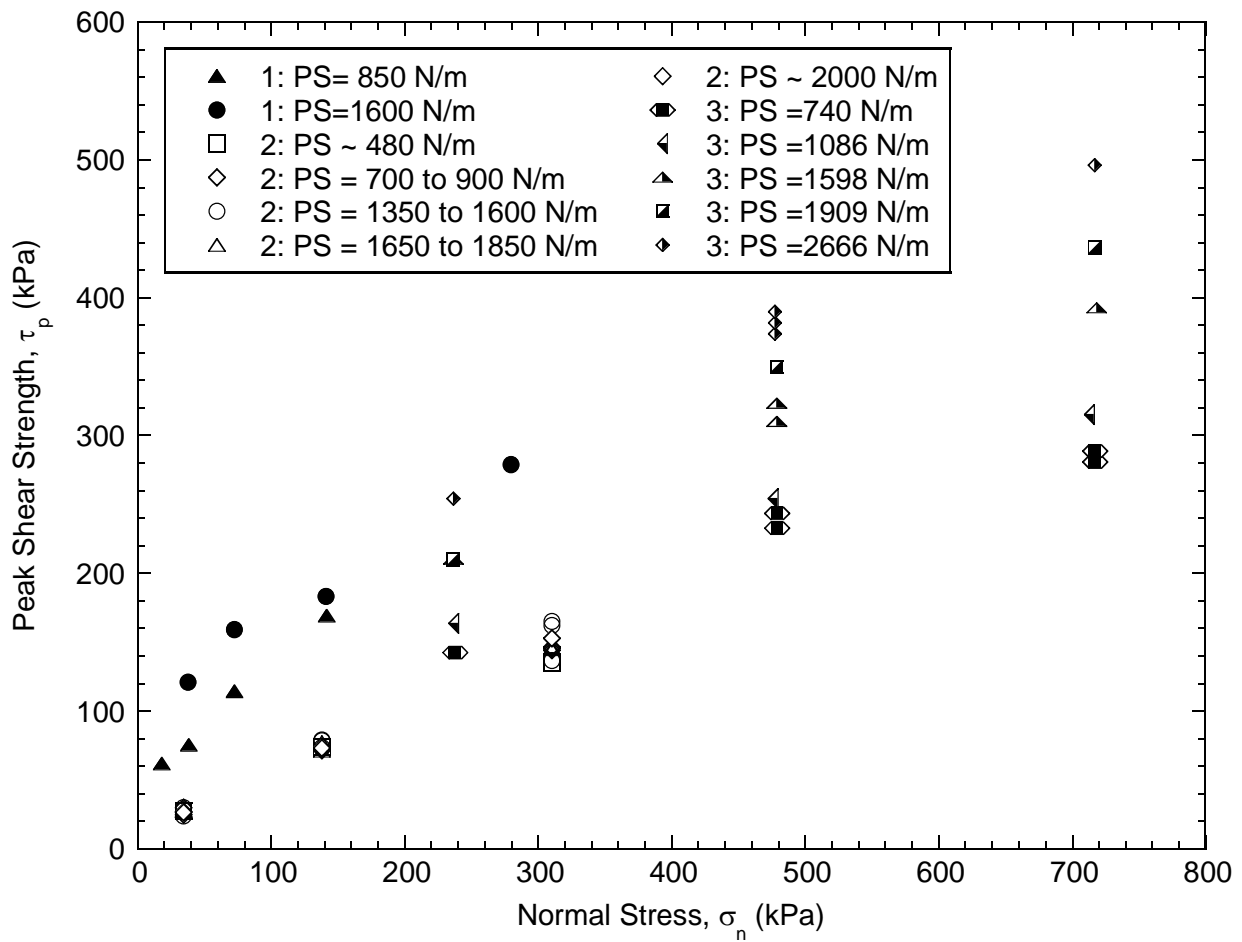


Fig. 2.7. Relationships of peak shear strength versus normal stress for a needle-punched reinforced geosynthetic clay liner (i.e., Bentomat ST) manufactured with a range of peel strengths (PS). References: 1 = Fox et al. (1998), 2 = Zornberg et al. (2005), and 3 = Athanassopoulou and Yuan (2011).

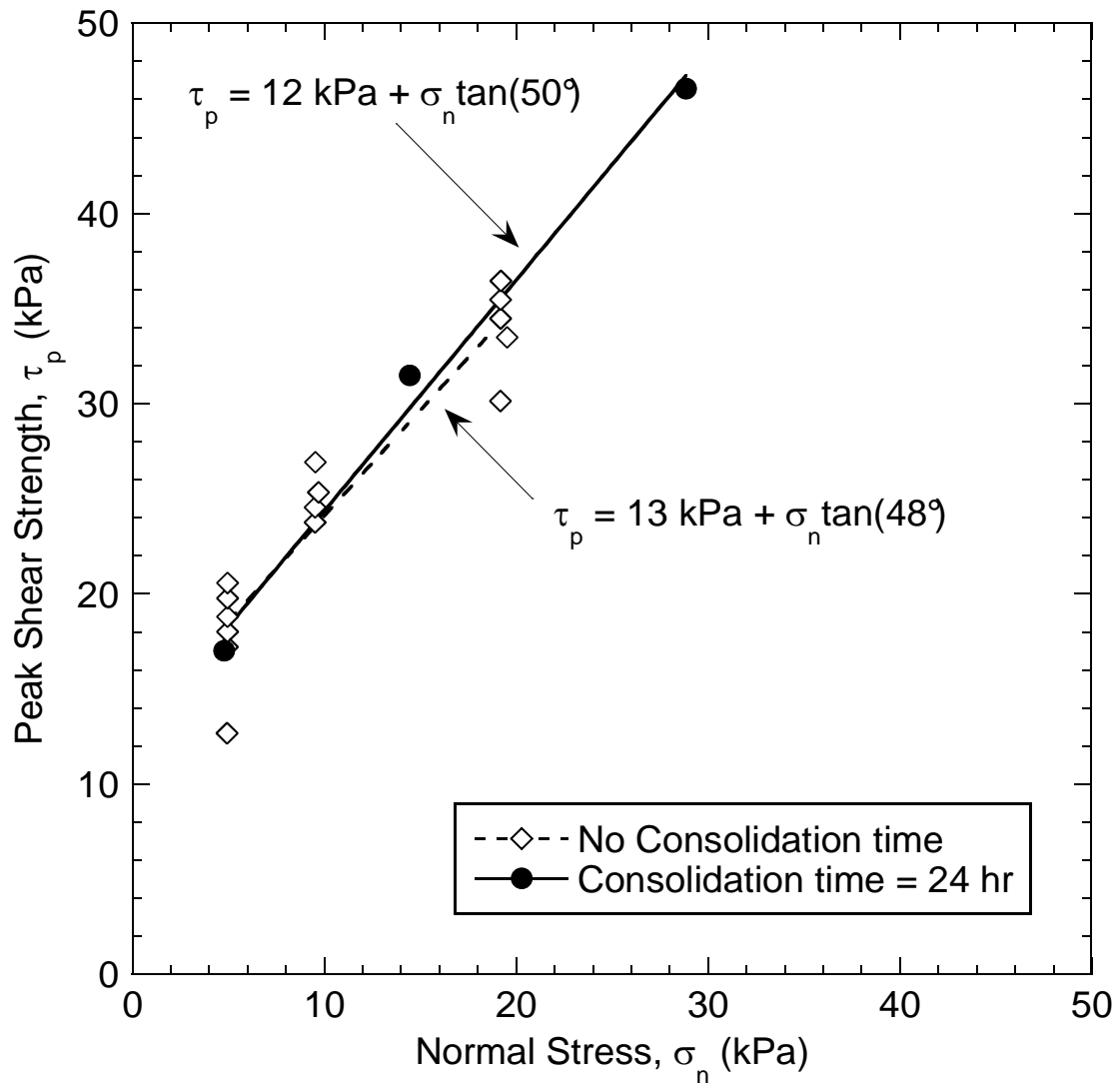


Fig. 2.8. Effect of consolidation on internal peak shear strength of a needle-punched reinforced geosynthetic clay liner (McCartney et al. 2009).

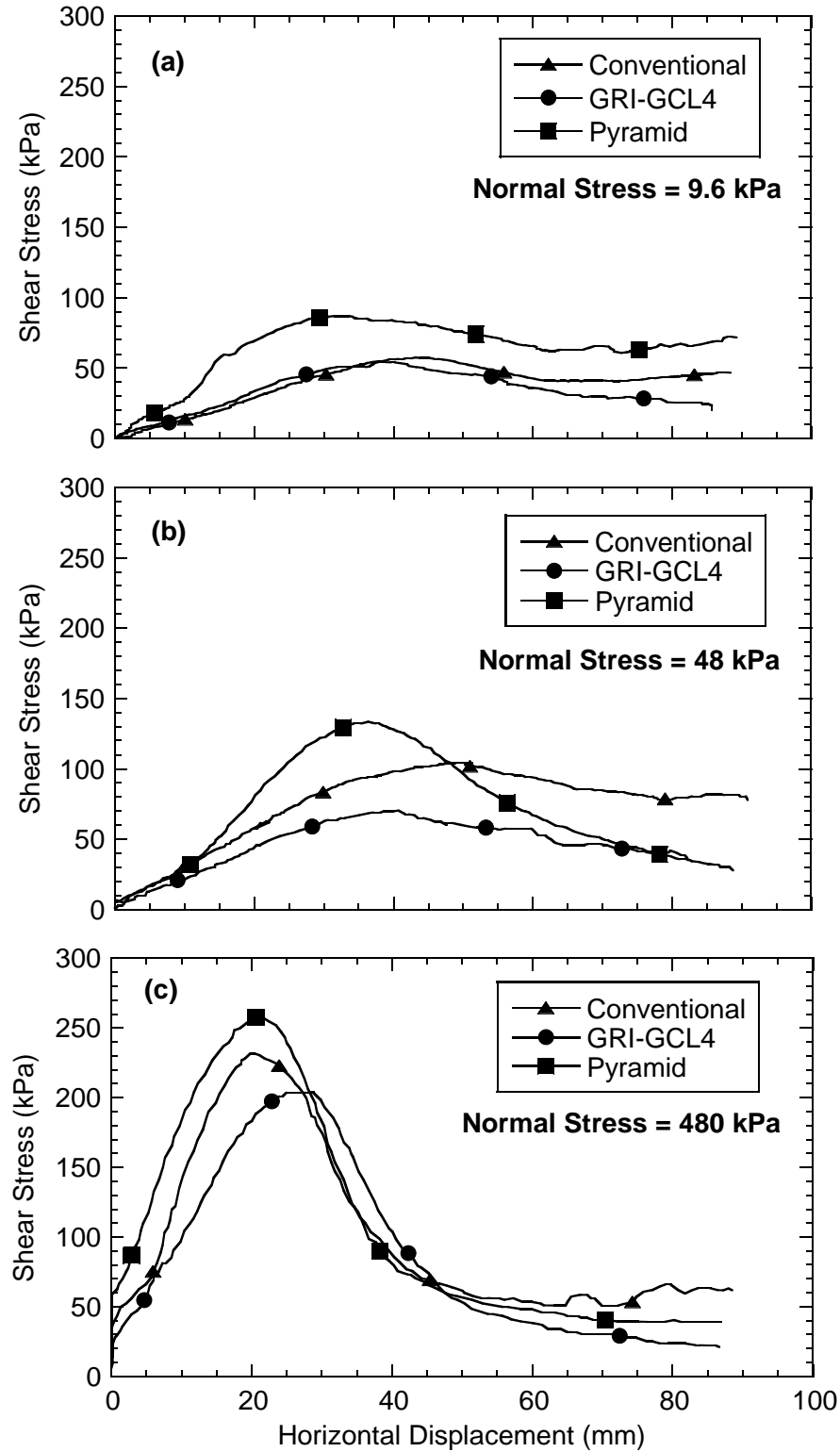


Fig. 2.9. Shear stress-displacement relationships from Allen and Fox (2007) for evaluation of different gripping surfaces. Experiments performed under (a)  $\sigma_n = 9.6$  kPa, (b)  $\sigma_n = 48$  kPa, and (c)  $\sigma_n = 480$  kPa.

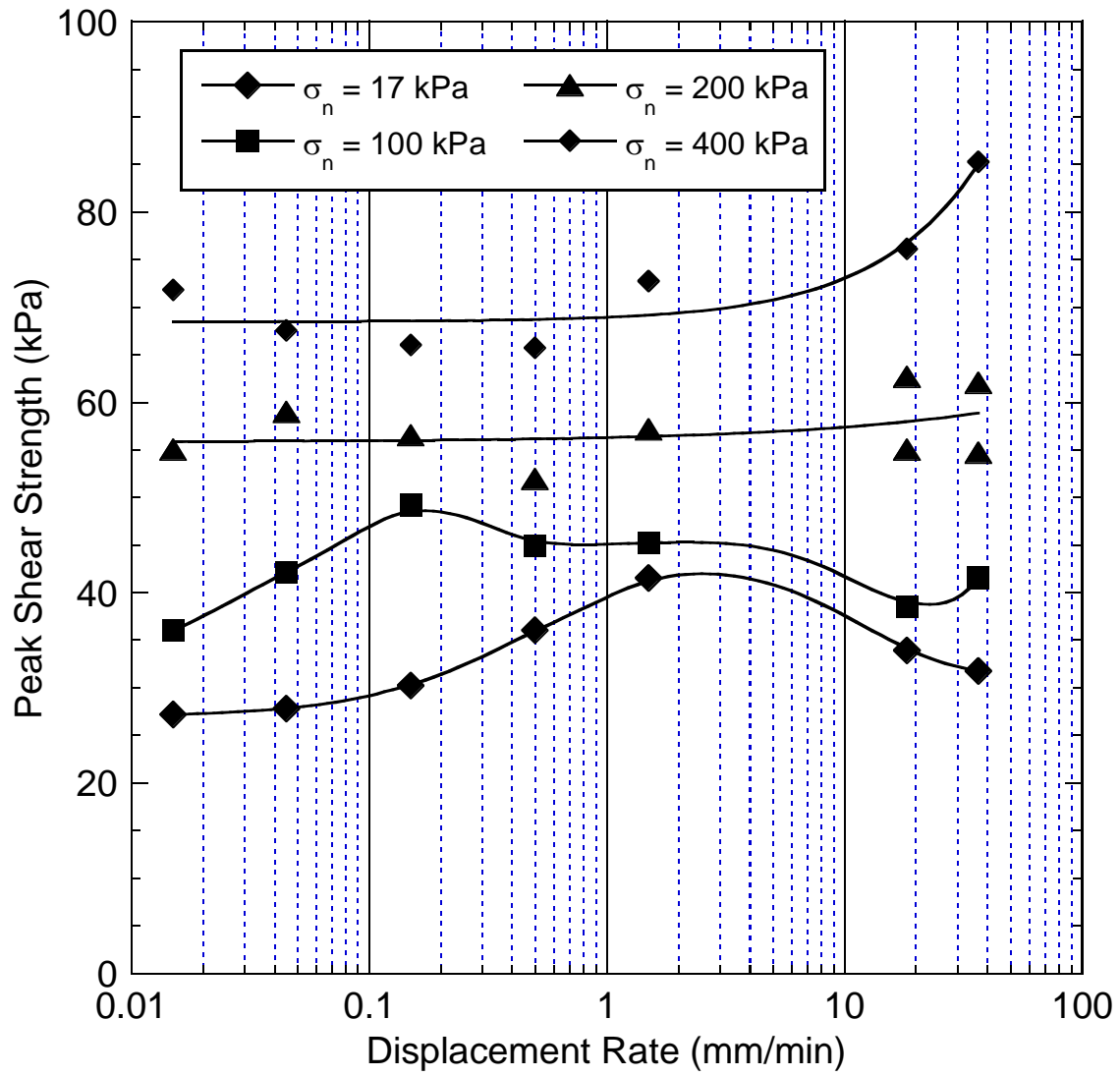


Fig. 2.10. Relationships of peak shear strength versus displacement rate for ring shear tests conducted on a thermally-bonded, needle-punched reinforced geosynthetic clay liner (Eid et al. 1999).

## CHAPTER 3: METHODS AND MATERIALS

### 3.1 Direct Shear Apparatus

A direct shear apparatus was developed to facilitate the following experimental conditions:

- Conduct displacement-controlled and stress-controlled direct shear experiments;
- Develop and maintain constant test temperatures up to 80°C;
- Incorporate 300-mm-square GCL specimens for  $\sigma_n$  up to 500 kPa and 150-mm-square GCL specimens for  $\sigma_n$  up to 2000 kPa; and
- Hydrate and expose GCLs throughout the duration of a shear experiment to non-standard chemical solutions (e.g., high ionic strength acidic and alkaline solutions).

Cross-section and plan-view schematics of the direct shear apparatus are shown in Fig. 3.1. A picture of apparatus is shown in Fig 3.2. The apparatus incorporated five main components: (i) normal force loading system, (ii) shear force loading system, (iii) external shear box, (iv) internal GCL shear box, and (v) data acquisition and control system.

#### 3.1.1 Normal Force Loading System

Normal force was generated via a 300-mm-diameter pneumatic air cylinder, which has been used successfully in previous work (e.g., Bareither et al. 2013). The air cylinder was fixed to two rectangular steel bars that were secured to the aluminum base plate via four 25-mm-diameter threaded rods. Normal force was applied to the top shear platen via a 102-mm × 102-mm square stainless steel loading plate (Fig. 3.1.a). During shear testing, the loading plate was secured to the top shear platen with four bolts to mitigate rotation of the upper shear platen and maintain a nearly horizontal GCL specimen throughout an experiment.

### 3.1.2 Shear Force Loading System

An Exlar FT45-0605 linear actuator powered via an electro servo motor was used to generate a horizontal force and push the external shear box (Fig. 3.1a). This linear actuator has a 150-mm stroke length to provide sufficient horizontal displacement to facilitate achieving both peak and large-displacement shear strengths. The servo motor was equipped with two inline gearheads to achieve horizontal displacement rates (DRs) from approximately 0.01 to 3.0 mm/min. The target DR for GCL internal shear strength tests was 0.1 mm/min based on recommendations in ASTM D6243 (2013) and Fox and Stark (2015). Thus, the range of DRs achievable with the linear actuator bound the target rate and provided flexibility to either decrease or increase the horizontal DR as needed.

The horizontal force applied to the external shear box with the linear actuator was transferred to a shear force across the GCL specimen via a reaction block and a 32-mm-diameter stainless steel shear loading rod fixed on the opposite end of the direct shear apparatus (Fig. 3.1a). The reaction block was fixed in place using a gusset plate and horizontal force load frame. The gusset plate was bolted to an aluminum base plate that was bolted to the steel table frame. The horizontal force between the linear actuator and reaction block was primarily dissipated between two 25-mm-diameter pre-tensioned steel rods (Fig. 3.1b).

The shear loading rod connected to the reaction block was used to apply horizontal force to the upper shear platen contained within the internal shear box (Fig. 3.1a). The shear loading rod was fixed at one end to the reaction block and passed freely through the external shear box via a linear bearing. Horizontal force was applied to the upper shear platen along a row of 29-mm-diameter stainless steel ball bearings connected to the shear loading rod (Fig. 3.1b). The ball bearings provided approximately 120 mm of linear contact between the shear load rod and top shear platen, and also allowed free vertical movement of the top shear platen to facilitate contraction or dilation of the GCL during shear. A 150-mm-wide stainless steel plate was

attached to the upper shear platen at the point of contact between the ball bearings connected to the shear load rod and top shear platen.

### *3.1.3. External Shear Box*

The external shear box was constructed of aluminum (outer dimensions = 648×457×254 mm and inner dimensions = 610×432×235 mm) and was designed to (i) be in direct contact with the horizontal load generated from the linear actuator, (ii) displace freely in the horizontal direction, and (iii) hold internal shear boxes that contained the GCL specimens (Fig. 3.1). A series of stacked steel plates was bolted to the external shear box at the location of contact with the piston of the linear actuator to absorb the point load. The piston of the linear actuator advanced horizontally at a controlled DR and the external shear box displaced freely in the horizontal direction via four ball-bearing carriages secured to bottom of the external shear box. These ball-bearing carriages slid along two stainless steel guiderails that were bolted to the aluminum baseplate (Fig. 3.1a).

On the side of the external shear box opposite the linear actuator, two partially-threaded aluminum rods passed through the lower half of the external shear box and served as a locking mechanism to hold the internal shear box in-place (Fig. 3.1b). These rods included a threaded end on the outside of the external shear box that allowed securing the rods in-place. The unthreaded portion of the rods passed through the external shear box with O-rings in-between the shaft of the rod and back-wall of the external shear box. Rectangular plates were attached to the inside end of the locking rods to push against the internal shear boxes.

### *3.1.4. Internal GCL Shear Boxes*

Internal shear boxes were constructed to accommodate a 300-mm × 300-mm square GCL specimen and a 150-mm × 150-mm square GCL specimen. A schematic of the 300-mm-square internal GCL shear box is shown in Fig. 3.3. Internal GCL shear boxes were constructed

from ultra-high-molecular-weight polyethylene (UHMW). The internal shear boxes were fabricated from UHMW due to corrosion resistance and insulation properties of this material, and were designed to facilitate shear testing of GCLs submerged in aggressive solutions and at elevated temperatures. Thus, the internal UHMW GCL shear boxes served as a corrosion-resistant reservoir for hydration solution, thermal insulator for elevated testing temperatures, and included a bottom shear platen that transferred horizontal force from the linear actuator to shear stress within the GCL test specimens.

Upper and lower shear platens for both the 300-mm and 150-mm internal shear boxes were constructed of UHMW. The lower shear platens were machined into the bottom of the external shear boxes, whereas the upper shear platens was a free-standing piece of UHMW that could be bolted to the normal force loading plate via intermediary stainless-steel plates bolted to the upper shear platens (Fig. 3.3). Thus, the upper shear platen was approximately fixed in a horizontal plane during shear testing, whereas the internal GCL shear box and lower shear platen were contained within the external shear box that was displaced horizontally during shear testing. The stationary nature of the upper shear platen and horizontal movement of the lower shear platen induced horizontal deformation and shear stress within GCL specimens that were sandwiched between the two shear platens.

As shear force was transferred to a GCL specimen during testing, tension developed in the reinforcement fibers within the NP-GCL generated a counter-clockwise moment. This moment acted to rotate the top shear platen and generated an upward force to the top platen. Rotation of the upper shear platen was mitigated via bolting the upper shear platen to the normal loading plate during shear testing. A constant normal force was maintained on the GCL specimen via a feedback control system (described subsequently) that integrated the air pressure regulated connected to the air cylinder and load cell used to measure the applied normal force on a GCL specimen.



Geosynthetic clay liner specimens were held against the upper and lower shear platens via pyramid-tooth gripping plates and clamping bars at opposite ends of the specimen (Fig. 3.3). Stainless steel pyramid-tooth gripping plates were developed based on designs presented in Allen and Fox (2007). Two sets of 300-mm-square pyramid-tooth gripping plates and two sets of 150-mm-square pyramid-tooth gripping plates were fabricated out of 16-mm-thick stainless-steel plates with different tooth heights to facilitate testing under a range of  $\sigma_n$ . One set of plates included 2-mm-tall pyramid-teeth with a 1 tooth/cm<sup>2</sup> pattern, whereas the other set of plates included 1-mm-tall teeth with a 2.7 tooth/cm<sup>2</sup> pattern. The 2-mm tooth plates were used for shear tests conducted at  $\sigma_n \leq 250$  kPa and the 1-mm tooth plates were used for shear tests conducted at  $\sigma_n > 250$  kPa. These tooth heights were based on recommendations in Allen and Fox (2007) as well as compression tests on representative GCL specimens such that during shear testing there would be no interference between the upper and lower pyramid-tooth plates. Stainless steel clamping bars were attached to opposite ends of the upper and lower pyramid-tooth plates and facilitated clamping GTs of the GCL to the upper and lower pyramid-tooth plates (Fig. 3.3).

A staggered step-pattern was machined into the shear platens and pyramid-tooth plates to serve as shear keys. These shear keys provided effective transfer of shear force to shear stress within the GCL test specimens and also allowed ease of installing, removing, and changing the pyramid-tooth plates. Drainage holes were drilled into the pyramid-tooth plates that aligned with drainage grooves machined into the shear platens. The drainage holes were 3.2-mm in diameter, and the drainage grooves were 3.2-mm wide and deep; both drainage holes and drainage grooves were machined on a square grid pattern. This drainage system was designed to promote even hydration of the GCL specimen prior to shear testing and allow free drainage during shearing.

### *3.1.5. Data Acquisition and Control System*

A data acquisition (DAQ) and control system for the direct shear apparatus was developed with the following design goals: (i) control horizontal DR or horizontal force via the linear actuator; (ii) control vertical force via the air cylinder; (iii) control elevated temperature of liquid in the internal GCL shear boxes via submersible heaters; and (iv) monitor horizontal and vertical force, horizontal and vertical displacement, air pressure applied to the air cylinder, and temperature of the solution during shear testing. The DAQ and control system included a personal computer, controller for the linear actuator, National Instruments compact DAQ system, and LabVIEW software. Horizontal force was measured with a low profile 44.5-kN load cell (1210AF-10K-B, Interface, Scottsdale, Arizona) and normal force was measured with a 66.7-kN S-type load cell (VLC-110, Virtual Measurement and Control, Santa Rosa, California). Vertical displacement was measured with two 50-mm linear-variable displacement transducers (LS1, Novotechnik, Southborough, Massachusetts, USA) and horizontal displacement was measured with a 150-mm linear potentiometer (TEX, Novotechnik, Southborough, Massachusetts, USA). Horizontal displacement was also monitored via revolutions of the servo motor used to control the DR of the linear actuator. Measurements for all sensors were collected every second and subsequently processed using a moving average technique.

Horizontal displacement was controlled via an AR-02AE Aries drive (Parker Hannifin Corporation, Rohnert Park, CA) connected to the linear actuator. Normal force was controlled via a feedback-controlled pressure regulator (QB-1, Proportion-Air, McCordsville, Indiana, USA) connected to the air cylinder. Temperature of the hydration solution was controlled via a solid-state relay switch connected to two cartridge heaters and type-T thermocouples that were submerged in the solution. All three control systems were monitored via LabVIEW and actual measurements of load or temperature were adjusted relative to target values.

The heating system included two cartridge heaters that were coated in a chemical and heat resistance epoxy, low-voltage motors connected to plastic stirring rods used to agitate the

solution, and thermocouples used to monitor and control temperature. The UHMW internal GCL shear box provided effective insulation on five sides of the hydration solution. The surface of the solution was covered with 10-mm-diameter, hollow polypropylene balls to provide insulation and minimize evaporation. Rigid polystyrene foam insulation was also placed over the surface of the internal shear box to provide additional insulation as needed.

Preliminary experiments were conducted to evaluate capability of the heating system to reach and maintain target elevated temperatures of 50 °C and 80 °C inside the internal shear box and within a GCL specimen. Thermocouples were placed within de-ionized (DI) water in the internal shear box to monitor and control temperature as well as within the bentonite layer of a GCL. Temporal relationships of temperature within the DI water in the internal shear box and within the GCL are shown in Fig. 3.4 for experiments on 300-mm and 150-mm specimens. There was a lag-time observed between the rise in temperature within the DI water and within the GCL specimen. A modestly higher control temperature for the hydration solution (2-4 °C above target temperature) was required to achieve a target temperature within the GCL. In all experiments shown in Fig. 3.4, the GCL specimen achieved the target test temperature within a maximum heating time of 15 h (900 min).

### **3.2. Materials**

Three GCLs tested as part of this study are summarized in Table 3.1. All GCLs needle-punched reinforces with no thermal bonding (Minerals Technology, CETCO®, Hoffman Estates, IL). The main GCL tested was Bentomat DN (GCL-A) with an average peel strength of 2170 N/m (ASTM D6496 2011). The other two GCLs tested included another Bentomat DN (GCL-B) with a higher peel strength of 2670 N/m and Bentomat CLT (GCL-C) with a peel strength of 1490 N/m. The Bentomat DN products included two non-woven geotextiles, whereas the Bentomat CLT included a woven and non-woven geotextile. Characteristics of the bentonite layer in the three GCLs were the same based on manufactured properties. Thus, the main

difference between the three GCLs was the magnitude of peel strength, where higher peel strength coincides with greater internal reinforcement between the two geotextiles.

### **3.3 Testing Procedure**

Internal shear strength testing of GCLs was conducted in accordance with ASTM D6243 (2013). Minor deviations were adopted as needed to adhere to the developed testing equipment and recommendations in literature (e.g., Fox and Stark 2015). The test procedure included the following steps: (i) specimen cutting, (ii) hydration, (iii) specimen setup in the apparatus, (iv) consolidation, and (v) shearing.

#### *3.3.1. Specimen Cutting*

All GCL test specimens were cut parallel to machine direction (i.e., direction of GCL placement on slopes) and tests were conducted in the machine direction to simulate field conditions. Specimens with initial dimensions of 150 mm × 203 to 229 mm were cut for 150-mm-square shear tests, and a 300 mm × 356 to 381 mm were cut for 300-mm-square shear tests. The longer dimension was in the machine direction to accommodate additional length needed to clamp the geotextiles to the pyramid-tooth plates (Fig. 3.3). Bentonite was removed from both ends of the longer dimension via cutting reinforcement fibers such that a 150-mm-square or 300-mm-square GCL specimen remained with intact reinforcement fibers.

#### *3.3.2 Specimen Hydration*

The standard hydration procedure adopted for use in the GCL shear experiments was developed via an initial test series on 150-mm-square GCL specimens to evaluate the effect of hydration on shear behavior and shear strength. A summary of five shear tests conducted with varying hydration procedure is in Table 3.2. Hydration of GCLs followed a 2-stage hydration procedure from Fox et al. (1998). Each of the two stages had a specific hydration normal stress

( $\sigma_{n-h}$ ) and elapsed time. In Fox et al. (1998), Stage 1 included hydration for 2 d under  $\sigma_{n-h} = 1$  kPa and Stage 2 included hydration for at least 2 d under the target  $\sigma_n$  for shear testing. In this study, Stage 1 included  $\sigma_{n-h} = 20$  kPa that was carried out for elapsed times of 2, 3, 5, and 7 d. After Stage 1, Stage 2 involved hydration for 1 d under the target  $\sigma_n$  for shear testing, which was 100 kPa for all experiments in the hydration procedure evaluation (Table 3.2). Hydration during Stage 1 was conducted in a plastic pan filled with DI water and GCLs were sandwiched between two layers of geocomposite (i.e., geonet adhered between two layers of GT). Stage 2 was conducted in the direct shear apparatus such that GCL specimens could continue hydrating and consolidate under  $\sigma_n = 100$  kPa. All specimens tested in the hydration procedure evaluation were sheared with a constant DR of 1 mm/min to a max displacement of at least 70 mm.

### 3.3.3. GCL Shear Testing

All GCL direct shear experiments followed a systematic procedure of hydration, specimen setup, consolidation, and shearing. A 2-stage hydration procedure was adopted for all specimens as described previously. The specimen setup involved placement of the GCL specimen between a set of pyramid-tooth plates and securing opposite ends of the geotextiles via clamping plates (Fig. 3.3). The pyramid-tooth plates and GCL specimen sandwiched between them was then transferred to the lower platen of the internal GCL box and subsequently the entire internal GCL shear box was placed into the external shear box (Fig. 3.1). The top shear platen with intermediary stainless steel plates was placed on top of the upper pyramid-tooth plate and the air cylinder piston was extended so that the normal loading plate just touched the upper shear platen. The normal loading plate was then bolted to the intermediary stainless steel plates. The shear loading rod was moved such that the ball bearings just touched the upper shear platen and then fixed in-place via locking nuts on both sides of the reaction block. Finally, the vertical and horizontal displacement transducers were

fixed in their respective positions (Fig. 3.1) and the internal GCL box was filled with DI water to inundate the GCL specimen.

The required  $\sigma_n$  for shear testing was applied incrementally to minimize bentonite extrusion from the GCL specimens. An initial  $\sigma_n = 20$  kPa was applied on the GCL and  $\sigma_n$  was increased via a load-increment-ratio of one such that  $\sigma_n$  on the specimen was doubled every 3 to 4 hr. Thus, to achieve a target  $\sigma_n$  of 100 to 2000 kPa for shear testing required 16 to 32 hr. After reaching the target  $\sigma_n$  for shear testing, test specimens were allowed to continue hydrating and consolidating under the applied target  $\sigma_n$  for at approximately 24 h prior to shearing.

A DR of 0.1 mm/min was used in all direct shear experiments to develop failure envelopes. Additional shear tests were conducted at a DR of 1 mm/min to evaluate the effect of hydration procedure and effectiveness of the pyramid-tooth plates on shear behavior and shear strength. All 150-mm GCL specimens were sheared to at least 70 mm of horizontal displacement and all 300-mm GCL specimens were sheared to at least 100 mm of horizontal displacement to effectively capture  $\tau_p$  and  $\tau_{ld}$ . Shear stresses and  $\tau_p$  and  $\tau_{ld}$  were computed with respect to the initial specimen area in the shear plane, which is in agreement with standard practice (e.g., Fox and Stark 2015). After shear testing, specimens were removed and visually inspected to assess failure and to measure final specimen dimensions. Six to eight bentonite samples were exhumed from GCL specimens following testing to measure bentonite water content along the center-line of the specimen (i.e., every 25 or 38 mm along the length of the 150-mm and 300-mm GCL specimens, respectively).

### **3.4 Repeatability of Experiments Conducted in the Large Direct Shear Apparatus**

Repeatability in the direct shear apparatus was evaluated using two sets of experiments performed on 150-mm-square specimens obtained from GCL-A under  $\sigma_n = 100$  kPa (Table 3.3). A summary of the experimental conditions and shear strength properties for these repeatability

tests is in Table 3.3. In the first set, two specimens were hydrated following the two-step hydration procedure from Fox et al. (1998). In the second set, another two specimens were hydrated in accordance with the two-step hydration adopted in this study (Sec. 3.3.2). All specimens were tested under  $\sigma_n = 100$  kPa, and each set of test specimens was cut from the same vicinity within the GCL sample roll. Cutting specimens from a close vicinity in a GCL sample roll aids in minimizing variability of peel strength between specimens.

Shear stress versus horizontal displacement relationships for both sets of repeatability tests are shown in Fig 3.5. All experiments exhibited anticipated shear stress versus horizontal displacement relationships, whereby shear stress increases to a peak and then reduced due to a loss of strength attributed to needle-punched reinforcement. Each set of repeatability tests reached similar values of shear stress at peak strength and all four experiments reach comparable values of large-displacement (Fig. 3.5 and Table 3.3). The small difference in shear behavior for displacements  $< 5$  mm is attributed to variability in pre-tensioning of interlocking fibers during Stage 1 hydration for  $\sigma_n = 1$  or 20 kPa. The difference in peak shear strength between the two sets of experiments was due to cutting the specimens from two different locations within the GCL sample rolls. The provided sample rolls from the manufacturer were cut across machine direction, which is likely to induce larger variation in peel strength as compared to specimens cut from the same path in the machine direction. Regardless of this variability, the close comparison of shear behavior between all experiments, similarity in peak strength for each set of repeatability tests, and similar among large-displacement strengths for all specimens supports the validity of internal shear behavior and shear strength of GCLs as measured in this new direct shear apparatus.

Table 3.1. Summary of geosynthetic clay liner material characteristics.

GCL Product Name	Carrier Geotextile	Cover Geotextile	Bentonite Characteristics <sup>a</sup>		Peel strength (N/m) <sup>b</sup>
			Mass per Area (kg/m <sup>2</sup> )	Swell Index (mL/2-g)	
GCL-A (Bentomat DN)	NW-Polypropylene 240 (g/m <sup>2</sup> )	NW-Polypropylene 283 (g/m <sup>2</sup> )	3.6	24	2180
GCL-B (Bentomat DN)	NW-Polypropylene 240 (g/m <sup>2</sup> )	NW-Polypropylene 283 (g/m <sup>2</sup> )	3.6	24	2670
GCL-C (Bentomat CLT) <sup>c</sup>	W-Polypropylene 150 (g/m <sup>2</sup> )	NW-Polypropylene 234 (g/m <sup>2</sup> )	3.6	24	1490

Note: *W* = woven; *NW* = non-woven

<sup>a</sup> Certified properties as reported by manufacturer

<sup>b</sup> Peel strength measured by manufacturer on sample rolls provided for this study

<sup>c</sup> Bentomat CLT had a adhered layer of textured geomembrane that was peeled off before shear testing



Table 3.2. Summary of shear tests conducted to evaluate the GCL hydration procedure.

Normal Stress: Stage 1 (kPa)	Hydration Time: Stage 1 (d)	Normal Stress: Stage 2 (kPa)	Hydration Time: Stage 2 (d)	Normal Stress at Failure (kPa)	Peak Shear Stress (kPa)	Secant Friction Angle at Peak (°)	Displacement to Peak (mm)	Shear Stress at 70 mm (kPa)
1	2	98.1	2	98.1	154	58	29.0	15.6
20	2	100.2	1	100.2	138.4	54	25.9	21.3
20	3	100.0	1	100.0	143.6	55	26.0	14.0
20	5	99.8	1	99.8	147.1	56	26.9	21.1
20	7	99.9	1	99.9	149.3	56	29.5	18.2

Table 3.3. Summary of shear tests conducted to evaluate repeatability.

Normal Stress: Stage 1 (kPa)	Hydration Time: Stage 1 (d)	Normal Stress: Stage 2 (kPa)	Hydration Time: Stage 2 (d)	Normal Stress at Failure (kPa)	Peak Shear Stress (kPa)	Secant Friction Angle at Peak (°)	Displacement to Peak (mm)	Shear Stress at 70 mm (kPa)
1	2	99.3	2	99.3	127.3	52	27.2	12.5
1	2	100.0	2	100.0	133.1	53	28.8	17.5
20	2	99.7	1	99.7	164	59	31.2	14.4
20	2	100.0	1	100.0	173	60	33.4	23.3



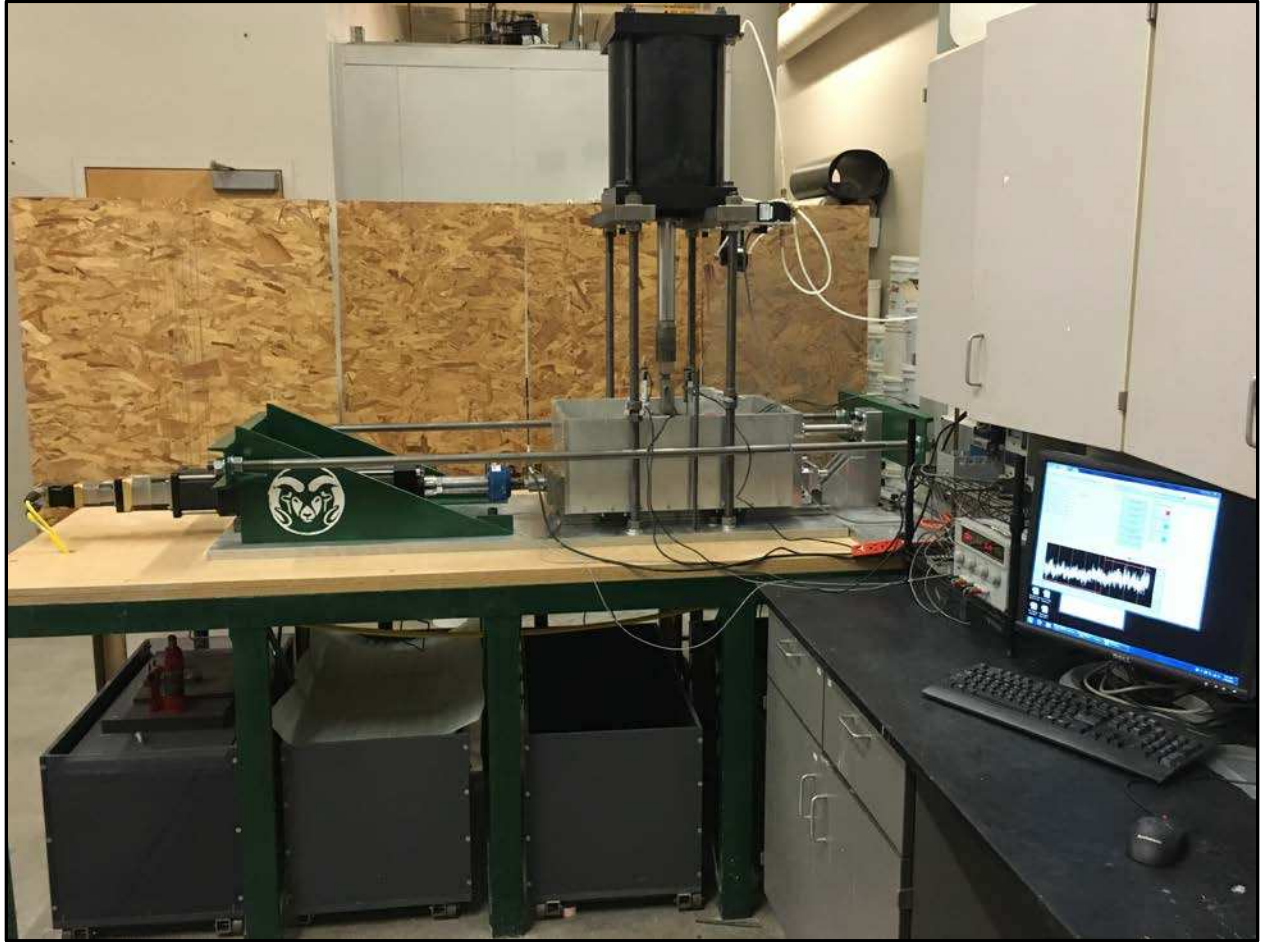


Fig. 3.2. Picture of direct shear apparatus with data acquisition system and personal computer.

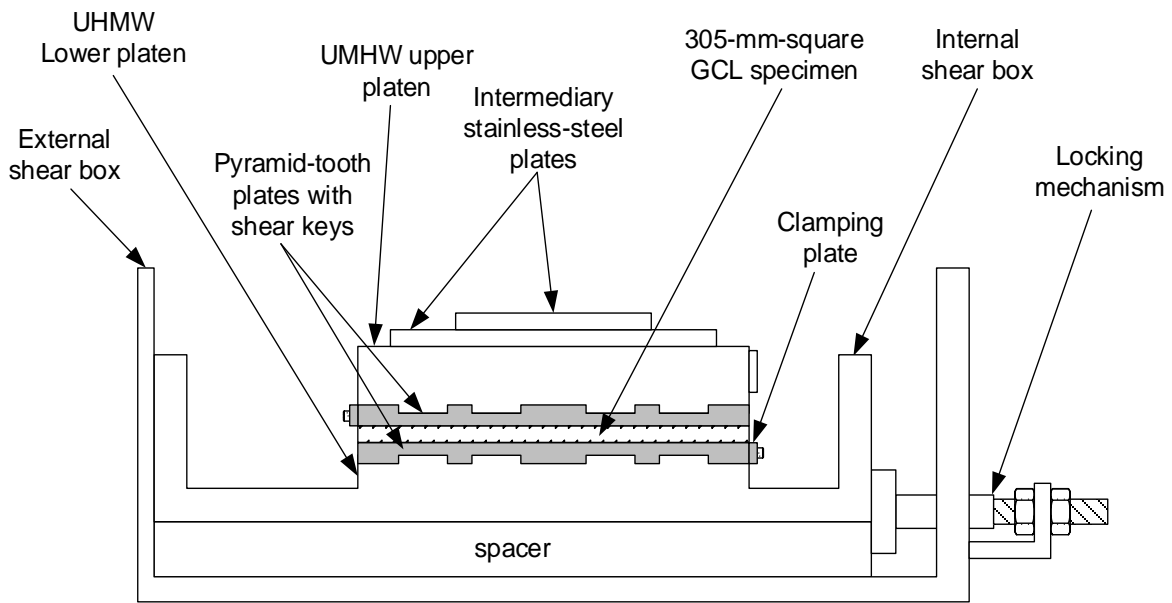


Fig. 3.3. Cross-section schematic of the 300-mm-square internal shear box that is positioned inside the external shear box for shear testing. Notes: GCL = geosynthetic clay liner; UHMW = ultra-high molecular weight polyethylene.

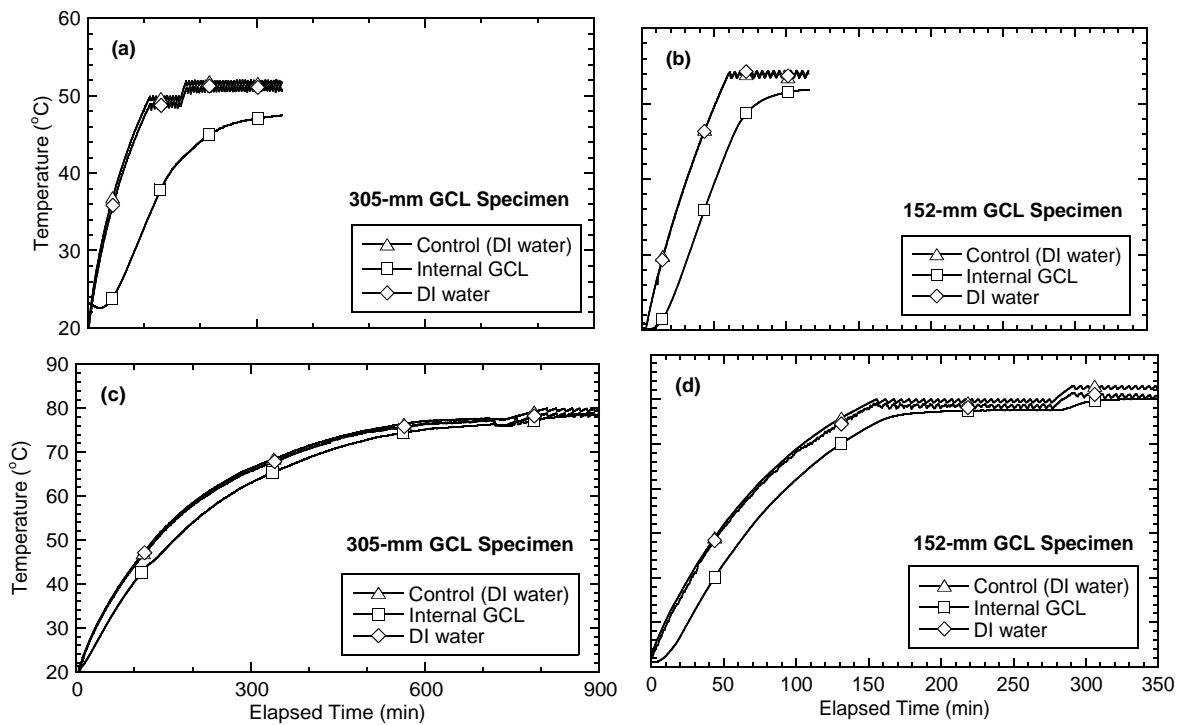


Fig. 3.4. Temporal relationships of temperature within the hydration solution and within the bentonite clay layer of a GCL for the following experiments: (a) 300-mm GCL heated to ~ 50 °C; (b) 150-mm GCL heated to ~ 50 °C; (c) 300-mm GCL heated to ~ 80 °C; and (d) 150-mm GCL heated to ~ 80 °C.

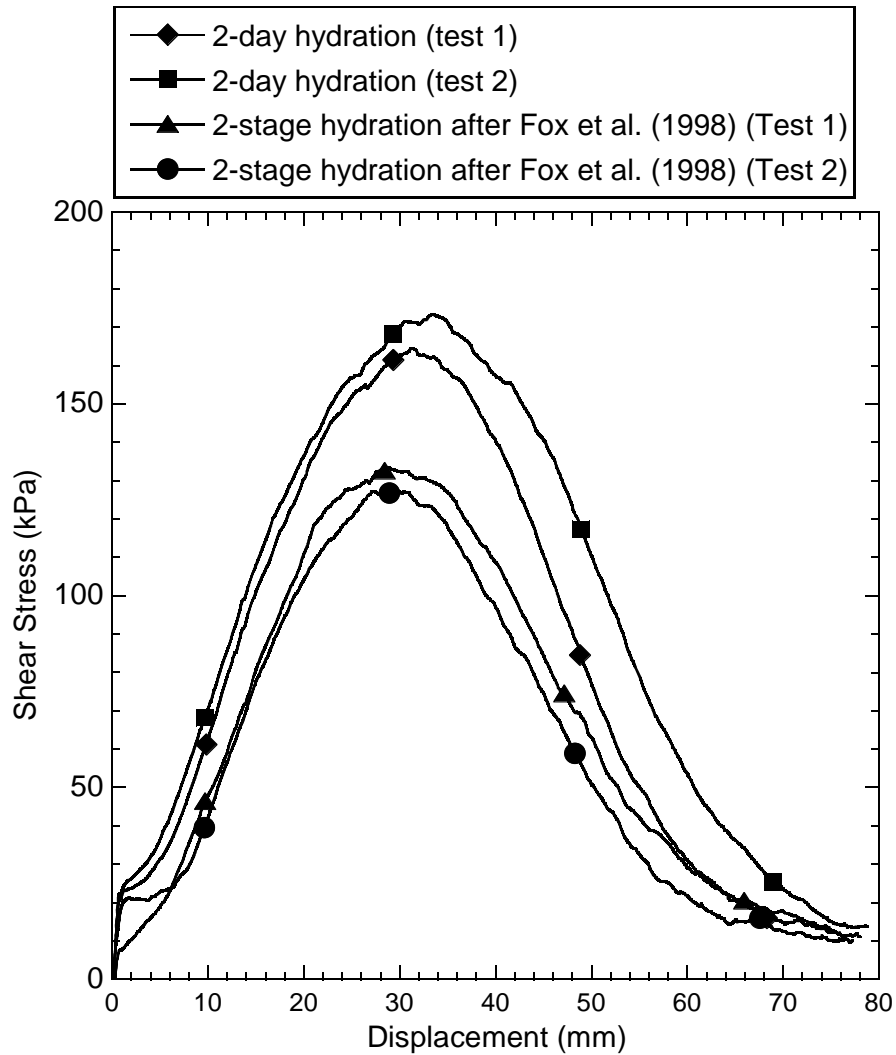


Fig 3.5. Relationships of shear stress versus horizontal displacement for two sets of experiments conducted to evaluate repeatability. Hydration conditions for these experiments are summarized in Table 3.3, and all experiments were conducted on 150-mm-square specimens of GCL-A at a normal stress of 100 kPa.

## CHAPTER 4: RESULTS AND DISCUSSION

A summary of fifteen direct shear experiments conducted as part of this study is in Table 4.1. Data compiled in Table 4.1 include specimen size, hydration normal stress ( $\sigma_{n-h}$ ) for Stage 1, normal stress during shear testing ( $\sigma_n$ ), peak shear stress ( $\tau_p$ ), secant friction angle at peak shear stress, horizontal displacement to peak shear stress, large-displacement shear stress ( $\tau_{ld}$ ), and average bentonite water content. The experiments compiled in Table 4.1 were conducted to (i) evaluate gripping surface effectiveness as a function of peel strength and  $\sigma_n$ , (ii) assess stress-displacement behavior for 150-mm and 300-mm GCL shear tests, and (iii) develop failure envelopes for  $\tau_p$  and  $\tau_{ld}$ . Additional direct shear experiments are compiled in Table 3.2 that were conducted to evaluate the effect of hydration procedure on internal shear behavior and shear strength of NP-GCLs.

### 4.1. Effectiveness of the Pyramid-Tooth Gripping Plates

#### 4.1.1 Influence of Normal Stress

Direct shear experiments were conducted on 150-mm-square GCL specimens at  $\sigma_n = 20, 50, 80,$  and  $100$  kPa to evaluate effectiveness of the pyramid-tooth gripping plates. Relationships of shear stress versus horizontal displacement for these four experiments are shown in Fig. 4.1a. All GCL specimens were hydrated using the 2-stage hydration method from Fox et al. (1998) and sheared at  $1$  mm/min to a horizontal displacement of at least  $70$  mm. Peak shear stress was not defined for the experiment conducted at  $\sigma_n = 20$  kPa due to slippage between the geotextiles and pyramid-tooth gripping surfaces, which led to development of tension within the GTs. However, a more pronounced peak shear stress can be observed with increase in  $\sigma_n$  (Fig. 4.1a). This behavior was attributed to more effective gripping between the GTs and pyramid-tooth plates as  $\sigma_n$  increased and more effective transfer



of horizontal force to internal shear force within the GCL. An  $\sigma_n = 100$  kPa was subsequently selected as the minimum  $\sigma_n$  for direct shear testing of GCL-A (Table 3.1) used in this study.

#### *4.1.2. Influence of GCL Peel Strength*

Relationships of shear stress versus horizontal displacement for three NP-GCLs with different peel strengths tested under  $\sigma_n = 100$  kPa are shown in Fig. 4.1b. The three NP-GCLs included GCL-A, GCL-B, and GCL-C (Table 3.1). All experiments were conducted on 150-mm GCL specimens that were hydrated following procedures in Fox et al. (1998) and sheared at 1 mm/min. A smooth stress-displacement relationship was observed for GCL specimens with peel strength of 1400 N/m and 2170 N/m (i.e., GCL-A and GCL-C), which indicates effective gripping between the pyramid-tooth plates and geotextiles of these two GCLs. Both of these experiments on the lower peel strength GCLs led to complete failure of the NP-reinforcement fibers based on identification of  $\tau_{id}$  and visual inspection of the GCLs post testing.

The general trend of increasing  $\tau_p$  with increasing peel strength observed for the three GCLs tested in this study (Fig. 4.1b and Table 4.1) has been observed in previous studies (e.g. Richardson 1997; Fox et al. 1998; Athanassopoulos and Yuan 2011). However, the GCL with peel strength = 2600 N/m (GCL-B) did not exhibit a smooth stress-displacement relationship and the experiment was stopped at approximately 40 mm of horizontal displacement due to slippage between the pyramid-tooth gripping plates and geotextiles of the GCL. The jagged stress-displacement behavior observed between 20 and 40 mm of horizontal displacement (Fig. 4.1b) coincides with specimen slippage along the gripping surface and tensile stress development within the cover GT (based on visual observation during testing and inspection post-testing). This observation indicates that the gripping surface effectiveness to internally shear a GCL specimen is dependent on the GCL type (e.g., peel strength) as well as  $\sigma_n$ .

A  $\sigma_n = 100$  kPa appeared to be a reasonable starting point for evaluating internal shear behavior and shear strength of GCLs for peel strength  $\leq 2200$  N/m. Additional lower  $\sigma_n$  can be added to a GCL testing program for lower peel strength GCLs. However, a lower-bound  $\sigma_n$  greater than 100 kPa should be used for testing GCLs with higher peel strength. An evaluation of a threshold  $\sigma_n$  for a given peel strength was only conducted for the GCL-A (peel strength = 2170 N/m); additional testing to evaluate a threshold  $\sigma_n$  for GCL-B and GCL-C was beyond the scope of this study.

#### **4.2. Evaluation of Hydration Procedure**

Relationships of shear stress versus horizontal displacement for shear tests conducted to evaluate the 2-stage hydration procedure (Table 3.2) are shown in Fig. 4.2. All tests revealed a comparable  $\tau_p$  and  $\tau_{id}$  regardless of hydration procedure, which is in agreement with McCartney et al. (2009) who reported no decrease in internal peak shear strength for NP-GCLs following 48 h of hydration under the same  $\sigma_n$  as the  $\sigma_n$  applied during shear. Also, comparability of  $\tau_p$  and  $\tau_{id}$  for all hydration tests summarized in Table 3.2 (Fig. 4.2) further supports repeatability of the direct shear apparatus.

A modest difference was observed in shear stress versus horizontal displacement behavior for the 2-stage hydration procedure that followed Fox et al. (1998). In this experiment, shear stress was lower relative to all other tests during initial horizontal displacement, which was due to increased tension within the reinforcement fibers during hydration under a lower Stage 1  $\sigma_n$ . Assuming a constant swell pressure on the bentonite clay in all experiments compiled in Table 3.2 and shown in Fig. 4.2, a lower  $\sigma_n$  would allow greater stress transfer to the reinforcement fibers during hydration, which likely elongated the fibers such that additional horizontal displacement was required to reach a similar shear stress during testing. However, regardless of the lower  $\sigma_n$  and potentially greater tensile stress in the reinforcement fibers

during hydration, all shear tests conducted to evaluate the 2-stage hydration yielded comparable shear behavior and internal shear strength. To avoid pre-tensioning reinforcement fibers prior to shearing, a 2-stage hydration with  $\sigma_n = 20$  kPa and at least 2 d of hydration for Stage 1 was adopted for experiments discussed in Section 4.4.

### 4.3. Shear Plane Area Correction

Relationships of area-corrected and non-area corrected (i.e., measured) shear stress and normal stress versus horizontal displacement for a 150-mm shear test conducted on GLC-A  $\sigma_n = 250$  kPa are shown in Fig 4.3. Data shown in Fig. 4.3 were evaluated to demonstrate an area correction procedure for GCL internal shear testing and were considered representative of GCL tests conducted as part of this study. Area corrections were applied to shear and normal stresses for each measurement based on the following formula:

$$\tau_c \text{ or } \sigma_{n,c} = \frac{F_{s,m} \text{ or } F_{n,m}}{(L_s - \delta_h) \times W_s} \quad (5)$$

where  $\tau_c$  = corrected shear stress,  $\sigma_{n,c}$  = corrected normal stress,  $F_{s,m}$  = measured shear force,  $F_{n,m}$  = measured normal force,  $L_s$  = specimen length,  $W_s$  = specimen width, and  $\delta_h$  = horizontal displacement. Continuous shear plane area reduction during testing led to a progressive increase in  $\sigma_{n,c}$  as well as larger corrected shear stresses for both  $\tau_p$  and  $\tau_{ld}$  (Fig. 4.3).

Peak shear stress developed during internal shear of a NP-GCL is predominantly due to pullout and tensile failure of reinforcement fibers and only a minor component of shear resistance can be attributed to shear strength of hydrated bentonite. This mechanism of peak shear stress resistance in NP-GCLs has been documented by others (e.g., references in Table 2.1) as well as in experimental data shown in Figs. 4.1 and 4.2. The initial shear plane surface area of a given NP-GCL specimen will contribute to peak shear resistance since reinforcement fibers can be assumed uniformly distributed over this initial surface. Uncorrected shear and

normal stresses based on the initial shear plane area shown in Fig. 4.3 yield a secant friction angle of 42.6°, whereas the area-corrected shear and normal stresses yield a secant friction angle of 43.0°. Although these secant friction angles are essentially the same, the mechanism of shear resistance in a NP-GCL suggests that the non-area corrected shear and normal stresses are more representative of peak shear stress conditions for internal failure of a GCL.

The pronounced loss in shear resistance of a NP-GCL following peak shear stress is due to complete pullout and/or rupture of reinforcement fibers. Continued horizontal displacement of the geotextiles relative to one another, eventually leads to a condition where shear resistance is a minimum and attributed primarily to hydrated bentonite (Fig. 4.3). The shear plane area at large-displacement (or residual) shear stress can be assumed more representative of the area-corrected consideration, which is computed as,

$$A_c = (L_s - \delta_h) \times W_s \quad (6)$$

where  $A_c$  = corrected shear plane area. Secant friction angles computed based on non-area corrected and area-corrected stresses for data in Fig. 4.3 are 9.0° and 7.8°, respectively. A modest decrease in secant friction angle was obtained by factoring in the area correction due to a more pronounced increase in  $\sigma_n$  relative to shear stress (Fig. 4.3).

A non-area corrected normal and shear stress analysis was adopted in this study for analysis of all GCL internal shear strength experiments. This analysis was believed appropriate due to (i) all reinforcement fibers within the initial shear plane area of a given specimen contributing to peak shear resistance and (ii) a modest difference between both peak and large-displacement secant friction angles. Furthermore, a review of literature (e.g., Table 2.1) suggests that shear plane area corrections have not been considered in past research on reinforced GCLs.

#### 4.4. Shear Stress-Displacement Relationships and Failure Envelopes

Relationships of shear stress and net vertical displacement versus horizontal displacement for 150-mm and 300-mm GCL shear tests are shown in Fig. 4.4. Experiments were conducted on 150-mm specimens for  $\sigma_n$  ranging from 100 to 2000 kPa and on 300-mm specimens for  $\sigma_n$  ranging from 100 to 500 kPa. A summary of failure stress conditions for all experiments is in Table 4.1. All shear tests exhibited anticipated shear behavior for NP-GCLs, whereby shear stress increased to a peak corresponding to  $\tau_p$  and then reduced and approached a shear stress representative of  $\tau_{id}$ . The amount of horizontal displacement for the 150-mm and 300-mm GCL specimens was sufficient to achieve a nearly constant large displacement shear stress (Fig. 4.4a and 4.4b) such that these  $\tau_{id}$  were considered representative of  $\tau_r$ .

A localized peak shear stress can be observed at horizontal displacements  $< 3$  mm. This behavior has been observed by others, and has been hypothesized as developing from insignificant slippage between the GCL and gripping plates before full gripping and transmission of shear force over the entire specimen area (Fox and Ross 2011). The authors believe this localized peak shear stress at small horizontal displacements is due to a transition from tensile deformation of needle-punched fibers to disentanglement of the fibers from the carrier geotextile. As shear stress develops on the surfaces of a the GCL with the intent to displace the cover and carrier geotextiles, this shear stress will transfer between the geotextiles as tensile stress within the reinforcement fibers. Initial shear stresses will be resisted by the tensile strength of the fibers until the point at which the tensile stress in the fibers exceeds the frictional strength where fibers are entangled in the carrier geotextile. The continued increase in shear stress measured in direct shear past the localized peak at small displacements is believed to be the mobilization of full frictional resistance of the reinforcement fibers.

Ultimately, a peak shear stress is reached where fibers begin to pullout or rupture from the carrier geotextile, which is followed by a progressive loss in shear stress.

Net vertical displacement plotted in Fig. 4.4c for 150-mm experiments and in Fig. 4.4d for 300-mm experiments represents the arithmetic average of vertical displacement measured at the front and back of a given test specimen (Fig 3.1a). The net vertical displacement measured in all GCL shear tests shown in Fig. 4.4 was contractive, which indicates the GCL thickness was decreasing during shear. A change in compressive behavior of the GCLs can be observed with additional horizontal displacement following the peak shear stress, whereby the rate of specimen contraction post-peak was nearly constant for a given experiment. This contractive behavior with continued shear displacement was attributed to a decreasing shear plane area that contributed to shear resistance following pullout and/or rupture of the reinforcement fibers (described previously). A continuous increase in normal stress with decreasing shear plan contact area (Fig. 4.3) likely contributed to the continuous contractive behavior observed in all GCL shear tests following attainment of a peak shear stress.

Failure envelopes representing peak and large-displacement shear strength ( $\tau_p$  and  $\tau_{ld}$ ) from the GCL shear experiments summarized in Fig. 4.4 are shown in Fig. 4.5. Data from Fox and Ross (2011) for experiments on a Bentomat DN NP-GCL with similar peel strength ( $\approx 2170$  N/m) also are included in Fig 4.5 for comparison. Peak shear strength data were represented with both a bilinear and nonlinear failure envelope (described previously in Section 2.3.2) to capture  $\tau_p$  for a broad range of  $\sigma_n$ . The bilinear failure envelope included two Mohr-Coulomb failure envelopes represented by Eqs. 7 and 8.

$$\tau_p = 137 \text{ kPa} + \sigma_n \tan 25.1^\circ \quad \text{for } 100 \leq \sigma_n \leq 500 \text{ kPa} \quad (7)$$

$$\tau_p = 299 \text{ kPa} + \sigma_n \tan 8.5^\circ \quad \text{for } 500 \leq \sigma_n \leq 2000 \text{ kPa} \quad (8)$$

The nonlinear model presented in Eq. 4 was fit to all peak shear strength data acquired from 150-mm and 300-mm shear tests conducted in this study. The nonlinear failure envelope shown in Fig. 4.4 for  $\tau_p$  is in Eq. 9.

$$\tau_p = 310 \text{ kPa} + \sigma_n \tan 8.2^\circ - \frac{266}{\left(1 + \frac{\sigma_n}{2077}\right)^{10.6}} \quad \text{for } 100 \leq \sigma_n \leq 2000 \text{ kPa} \quad (9)$$

These bilinear and nonlinear failure envelopes effectively capture all data obtained from this study as well as provide a reasonable estimate of the GCL internal peak shear strength reported in Fox and Ross (2011).

A single Mohr-Coulomb failure envelope was sufficient to capture  $\tau_{id}$  (Fig. 4.5). Single  $\tau_{id}$  failure envelopes were developed for 150-mm GCL specimens based on shear stress at horizontal displacement = 70 mm and for 300-mm GCL specimens based on shear stress at horizontal displacement = 100 mm. These  $\tau_{id}$  failure envelopes are presented in Eqs. 10 and 11.

$$\tau_p = 21 \text{ kPa} + \sigma_n \tan 2.9^\circ \quad \text{for } 100 \leq \sigma_n \leq 2000 \text{ kPa (150-mm specimens)} \quad (10)$$

$$\tau_p = 2.3 \text{ kPa} + \sigma_n \tan 5.9^\circ \quad \text{for } 100 \leq \sigma_n \leq 500 \text{ kPa (300-mm specimens)} \quad (11)$$

Peak shear strengths for the first portion of the bilinear and nonlinear failure envelopes in this study are slightly greater than those reported in Fox and Ross (2011). These differences may be due to specimen variability, difference in gripping surface, or specimen conditioning since experiments at lower  $\sigma_n$  are more sensitive to these variables. However,  $\tau_p$  measured for 150-mm GCL specimens in this study at 1000 and 2000 kPa align well with data from Fox and Ross (2011) and support the accuracy of the developed shear apparatus to measure peak internal shear strength of GCLs. The  $\tau_{id}$  measured in this study and  $\tau_{id}$  reported by Fox and Ross (2011) are also comparable with only modest differences as a function of  $\sigma_n$ . The failure envelope for  $\tau_{id}$  based on stress in the 300-mm GCL specimens essentially passes

through the origin and can be assumed more representative of residual shear strength since additional horizontal displacement leads to near complete pullout and/or rupture of reinforcement fibers.

The  $\tau_p$  and  $\tau_{ld}$  data compiled in Fig. 4.5 for GCL shear tests conducted with the direct shear apparatus developed for this study as well as data from Fox and Ross (2011) represent three different size GCL direct shear tests specimens. Experiments from Fox and Ross (2011) were conducted on 305 mm by 1067 mm NP-GCL specimens with a maximum horizontal displacement of 200 mm to capture residual strength (Table 2.1). The close comparison between  $\tau_p$  and  $\tau_{ld}$  for both 150-mm and 300-mm GCL shear tests in this study and Fox and Ross (2011) for the broad range of  $\sigma_n$  shown in Fig. 4.5 suggest that smaller-sized GCL specimens can capture internal shear behavior and shear strength of NP-GCLs.

Horizontal displacement to  $\tau_p$  for 150-mm-square and 300-mm square specimens are shown in Fig. 4.6. The displacement to  $\tau_p$  for 150-mm specimens decreased with an increase in normal stress from 26 mm for  $\sigma_n = 100$  kPa to 21 mm for  $\sigma_n = 500$  kPa and was comparable for experiments performed at  $\sigma_n > 500$  kPa (Table 4.1). Comparable displacements to  $\tau_p$  were observed for 300-mm specimens. However, a slightly larger displacement to  $\tau_p$  was measured for the 300-mm shear test conducted at  $\sigma_n = 250$  kPa. The different was believed to be insignificant to overall shear behavior and shear strength and was attributed to variability in specimen properties (e.g., peel strength) between multiple specimens obtained from a single GCL roll cut across machine direction. Overall, the shear behavior observed in this study (e.g., Fig. 4.4) for the new direct shear apparatus is comparable to previously reported internal shear behavior of GCLs (e.g., Fox and Stark 2004).



Table 4.1. Summary of geosynthetic clay liner direct shear experiments conducted as part of this study to evaluate internal shear strength.

Specimen Width (mm)	Hydration Normal Stress for Stage 1 (kPa)	Shearing Normal Stress (kPa)	Peak Shear Stress (kPa)	Secant Friction Angle at Peak Shear Stress (°)	Horizontal Displacement to Peak Shear Stress (mm)	Shear Stress at 70 or 100 mm (kPa) <sup>a</sup>	Average Bentonite Water Content (%)
150	1.0	18.9	-	-	-	-	165
150	1.0	50.0	115.8	67	35.8	43.9	156
150	1.0	79.5	149.1	62	28.9	12.7	190
150	1.0	98.1	154.0	58	29.0	15.6	138
150 <sup>b</sup>	1.0	98.1	106.7	47	25.45	9.8	216
150	1.0	98.1	154.0	58	29.6	15	138
150 <sup>c</sup>	1.0	99.6	-	-	-	-	169
150	20	100.7	166.2	59	26.2	33.0	131
150	20	251.7	238.7	43	23.9	34.6	112
150	20	500.0	381.8	37	21.3	50.5	56
150	20	998.3	435.2	24	21.4	71.7	63
150	20	1954	594	17	21.4	116.5	49
300	20	100.0	165.9	59	26.4	13.7	130
300	20	251.4	273.4	47	28.7	26.9	126
300	20	499.7	359.6	36	26.1	54.8	75

<sup>a</sup> Shear stress at 70 mm of horizontal displacement for 150-mm specimens and shear stress at 100 mm for 300-mm specimens

<sup>a</sup> Bentomat CLT with peel strength  $\approx$  1400 N/m (GCL-C in Table 3.1)

<sup>b</sup> Bentomat DN with peel strength  $\approx$  2600 N/m (GCL-B in Table 3.1)

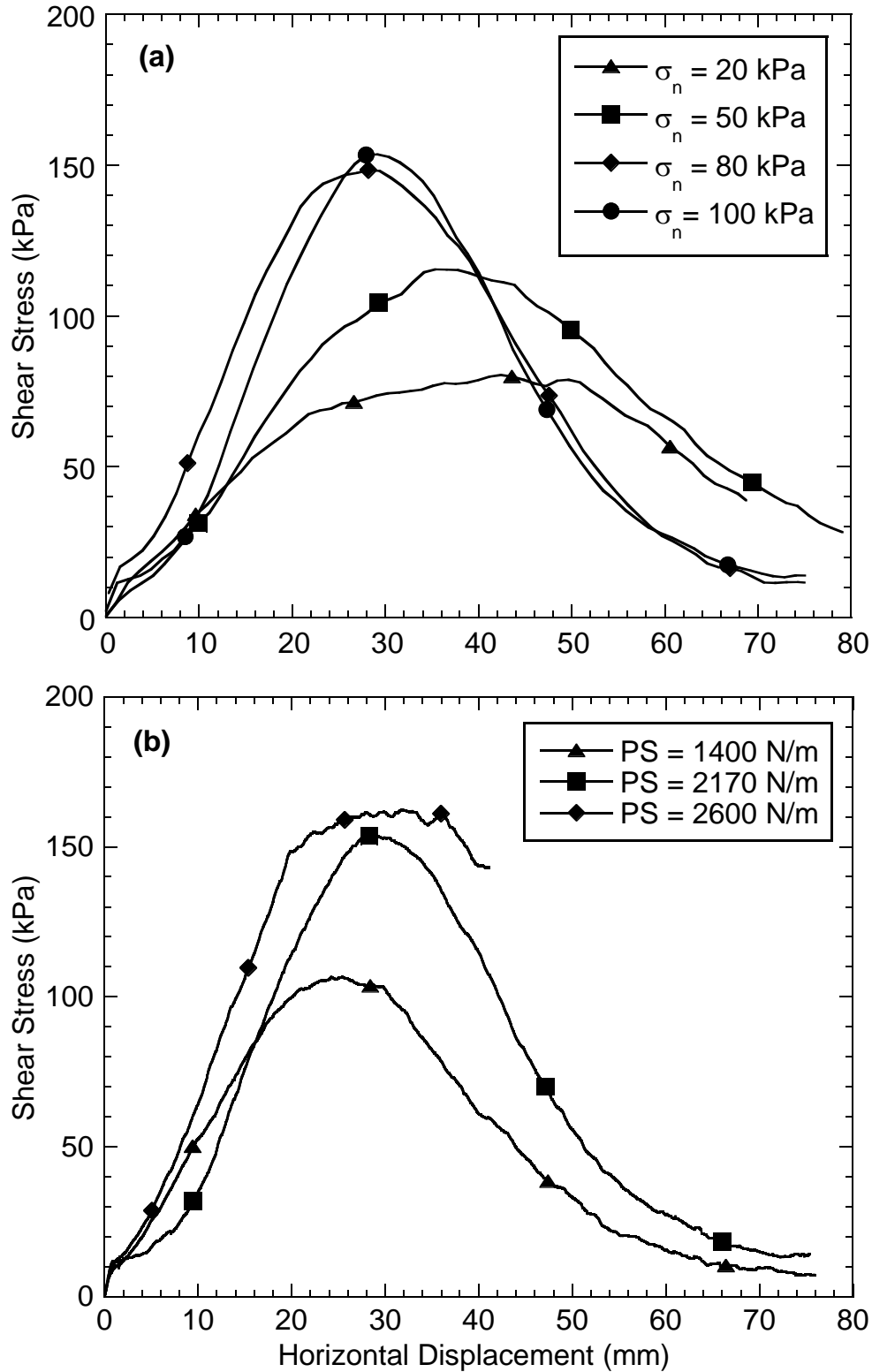


Fig. 4.1. Relationships of shear stress versus horizontal displacement for 150-mm-square GCL specimens conducted to evaluate the effectiveness of the pyramid-tooth plates versus (a) normal stress and (b) peel strength of specimen.

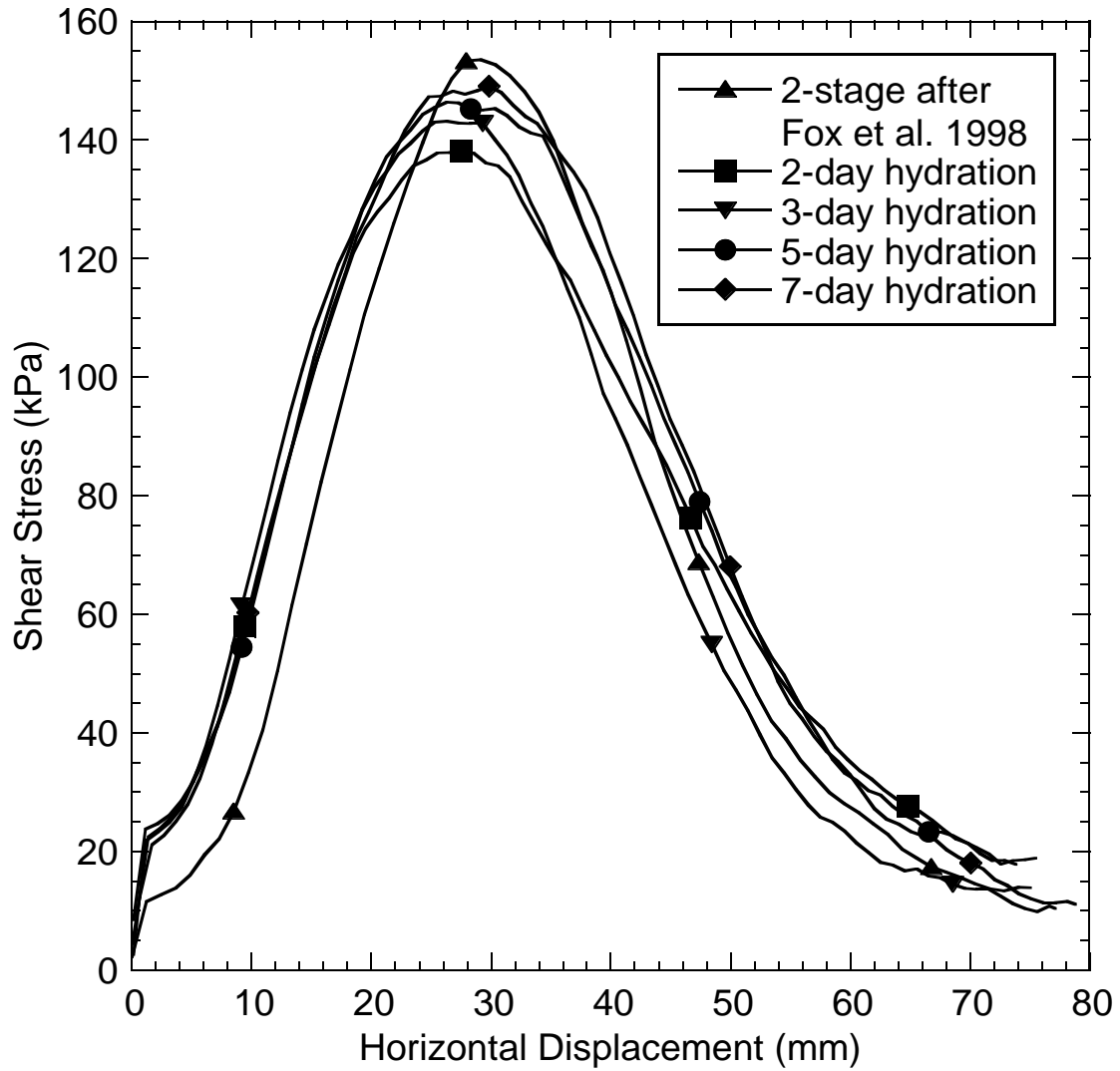


Fig. 4.2. Relationships of shear stress versus horizontal displacement for 150-mm-square GCL specimens conducted to evaluate 2-step hydration procedures.

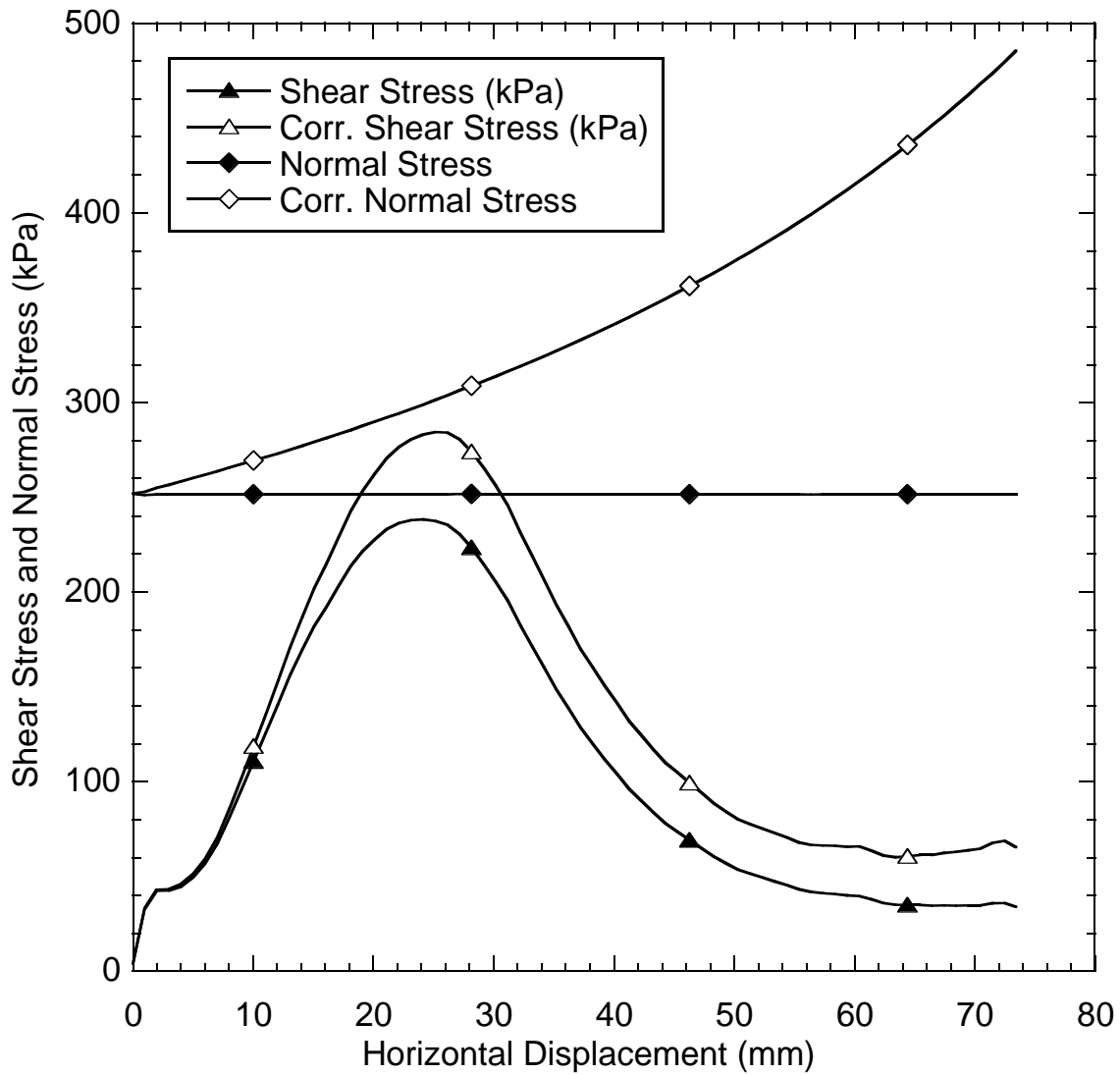


Fig. 4.3. Relationships of shear stress and normal stress versus horizontal displacement for considerations of no-area correction applied during shear and corrected shear and normal stress based on a reducing shear plane area. Example data are shown for a direct shear test conducted on a 150-mm specimen.

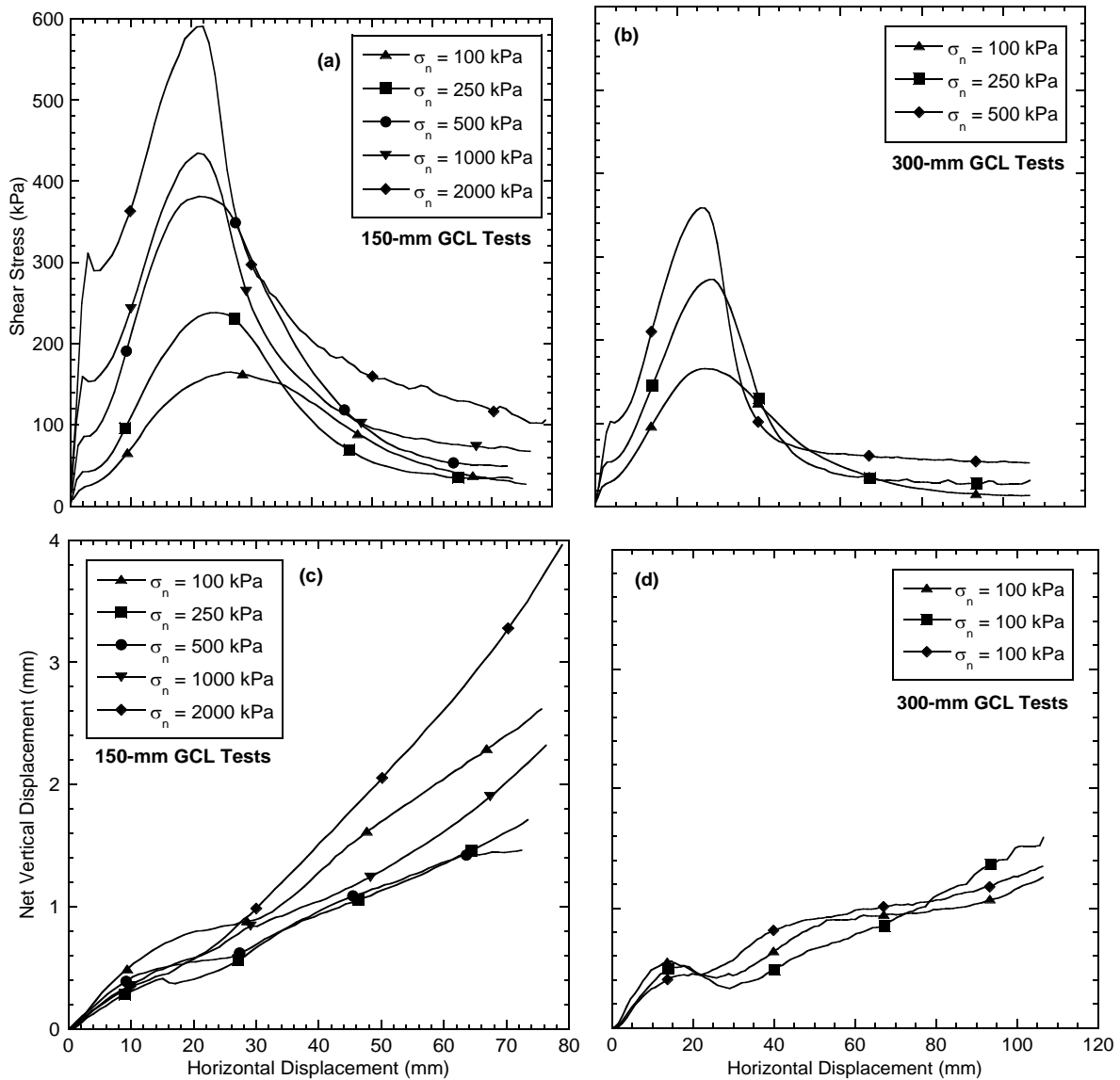


Fig. 4.4. Relationships of shear stress and net vertical displacement versus horizontal displacement for shear tests conducted: (a) shear stress for 150-mm specimens, (b) shear stress for 300-mm specimens, (c) vertical displacement for 150-mm specimens, and (d) vertical displacement for 300-mm specimens.

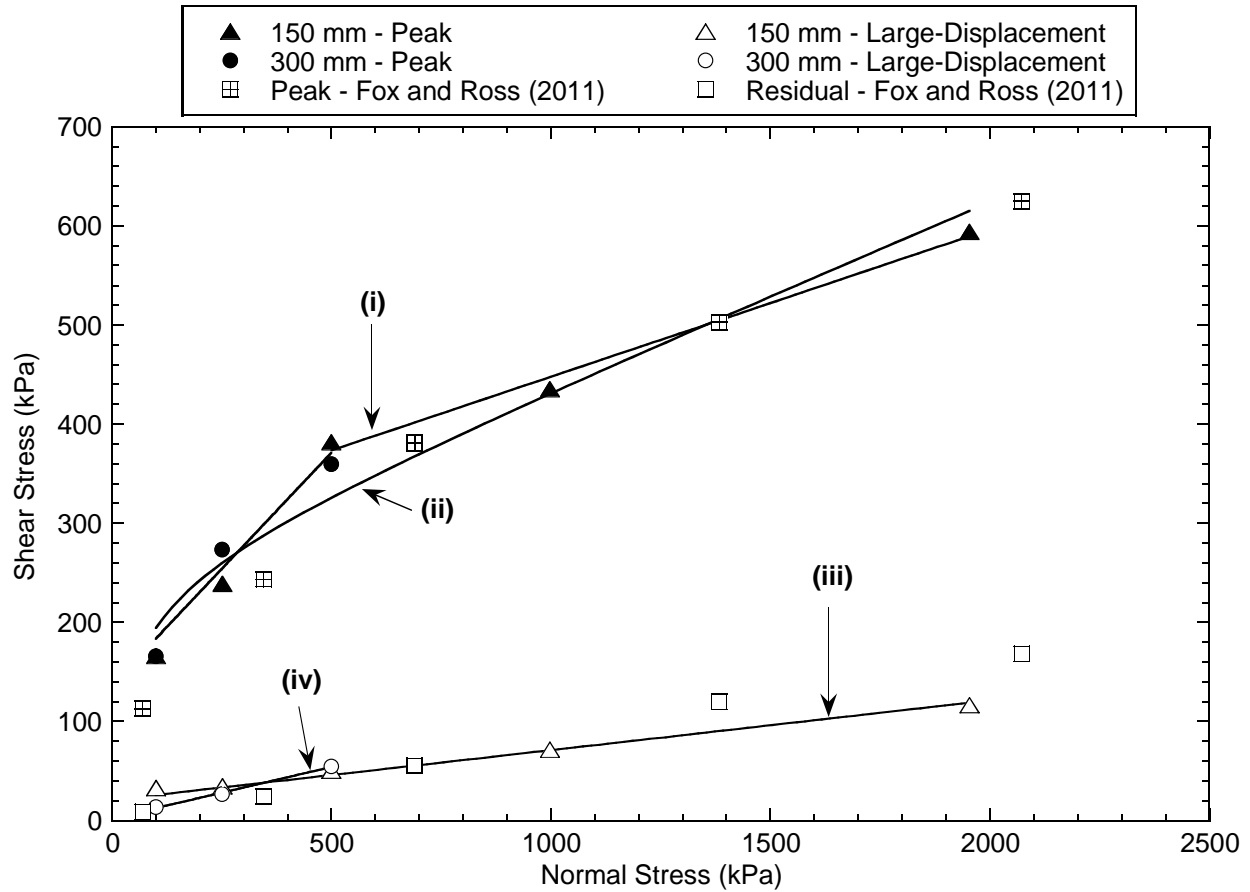


Fig. 4.5. Peak and large-displacement failure envelopes for the needle-punched reinforced GCL tested in this study. Data from Fox and Ross (2011) are for a comparable GCL. Failure envelopes shown in the plot: (i) bilinear, peak shear strength failure envelope for 150- and 300-mm GCL tests with one failure envelope for  $\sigma_n \leq 500$  kPa and one for  $\sigma_n \geq 500$ ; (ii) nonlinear, peak shear strength failure envelope for 150-mm and 300-mm GCL tests; (iii) linear, large-displacement shear strength failure envelope for 150-mm GCL shear tests based on shear stress at horizontal displacement = 70 mm; and (iv) linear, large-displacement shear strength failure envelope for 300-mm GCL shear tests based on shear stress at horizontal displacement = 100 mm large-displacement shear strengths.

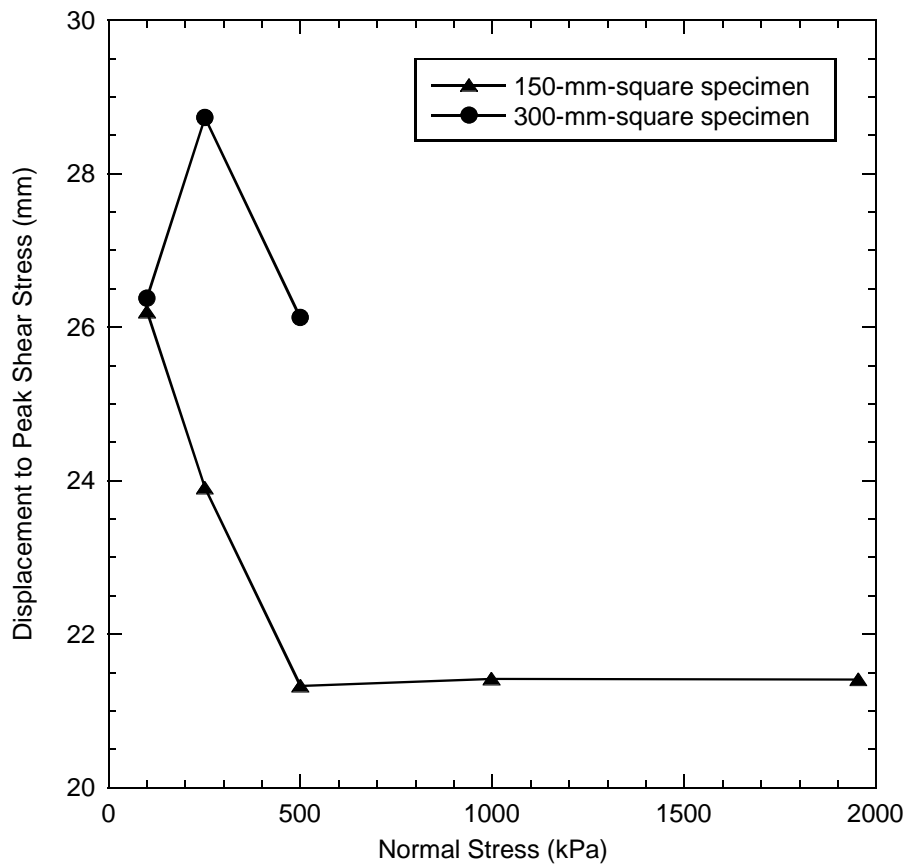


Fig 4.6. Relationships of displacement to peak shear stress versus normal stress for shear tests conducted on 150-mm and 300-mm specimens.

## CHAPTER 5: CONCLUSIONS AND FUTURE WORK

### 5.1 Conclusions

A novel direct shear apparatus was developed to evaluate internal shear strength of GCLs for mining applications. Experiments were conducted to assess effectiveness of the gripping surface under low normal stress and appropriateness of hydration procedures. Also, a series of shear tests were conducted on 150-mm-square and 300-mm-square GCL specimens to develop peak and large-displacement failure envelopes to compare with a previous study and validate the direct shear apparatus and experimental procedure. The following conclusions were drawn from this study.

- Effectiveness of the pyramid-tooth gripping plates increased as normal stress increased from 20 to 100 kPa. Under very low normal stresses, shear force was partially transferred to tensile force within the geotextiles of the GCL due to insufficient contact and possible slippage between the geotextiles and gripping surface. Clear definition of peak shear strength was attained for normal stress = 100 kPa for the reinforced NP-GCL with peel strength of 2170 N/m.
- Peel strength of NP-GCLs influenced effectiveness of the gripping surface under a normal stress of 100 kPa. Two NP-GCLs with peel strengths of 1400 N/m and 2170 N/m were successfully sheared. A GCL with peel strength of 2670 N/m exhibited tensile force development within the geotextiles during shearing at the same 100 kPa normal stress. This behavior was attributed to slippage between the geotextiles and pyramid-tooth gripping surfaces due to the higher peel strength.
- A series of 2-stage hydration tests indicated that hydration under a low normal stress (1 to 20 kPa) for 2 d followed by step-wise incremental loading to the prescribed normal stress for shear and an additional 1 d of hydration is appropriate to effectively measure



internal shear strength of a NP-GCL. Longer hydration times up to 7 d under a low hydration normal stress did not influence internal GCL shear strength.

- Peak shear strength was simulated with a bilinear and a nonlinear failure envelope to capture the internal shear strength of the reinforced GCL for normal stress ranging from 100 to 2000 kPa, whereas large-displacement strength were simulated with a single, linear failure envelope. Peak and large-displacement shear strengths compared favorably to a previous study on a NP-GCL with similar peel strength. This comparison validated the ability of the new direct shear apparatus to effectively measure internal shear behavior and shear strength of NP-GCLs.
- Peak and large-displacement shear strength measured on NP-GCLs for two different sized specimens in this study (150-mm square and 300-mm square) compared favorably to one another as well as with shear strength measured on a similar GCL with larger test specimens (305 mm x 1067 mm). These comparisons indicate that small-sized shear tests can yield accurate measures of shear behavior and shear strength for NP-GCLs.

## **5.2 Future Work**

The current research focused on developing a direct shear apparatus to evaluate shear strength of GCLs for use in mining application. Future research should be conducted to evaluate the effects of temperature and non-standard hydration solution on shear behavior and shear strength of GCLs. Additionally, internal shear strength should be conducted on GCLs exposed to non-standard hydration solutions and/or elevated temperatures for extended periods of time prior to testing. These aforementioned tests will yield insights into the effects of non-standard hydration solutions and temperature on internal shear strength of GCLs to aid in design of waste containment systems for mining applications.

## REFERENCES

- Allen, J. M. and Fox, P. J. (2007). Pyramid-tooth gripping surface for GCL shear testing. *Geosynthetics '07*, North American Geosynthetics Society, Washington, DC, (CD-ROM).
- ASTM. (2002). Standard test method for fluid loss of clay component for geosynthetic clay liner. ASTM D5891/D5891M-02, ASTM International, West Conshohocken, Pennsylvania, USA.
- ASTM. (2002). Standard test method for fluid loss of clay component for geosynthetic clay liner. ASTM D5891/D5891M-02, ASTM International, West Conshohocken, Pennsylvania, USA.
- ASTM. (2004). Standard test methods for determining average bonding peel strength between top and bottom layers of needle-punched geosynthetic clay liners. ASTM D6496/D6496M-04a, ASTM International, West Conshohocken, Pennsylvania, USA.
- ASTM. (2009). Standard Test Method for Measurement of Index Flux Through Saturated Geosynthetic Clay Liner Specimens Using a Flexible Wall Permeameter. ASTM D5887-09, ASTM International, West Conshohocken, Pennsylvania, USA.
- ASTM. (2010). Standard test methods for liquid limit, plastic limit, and plasticity index of soils. ASTM D4318-10, ASTM International, West Conshohocken, Pennsylvania, USA
- ASTM. (2011). Standard Practice for Quality Control of Geosynthetic Clay Liners. ASTM D6496/D6496M-04a, ASTM International, West Conshohocken, Pennsylvania, USA.
- ASTM. (2011). Standard test method for swell index of clay mineral component of geosynthetic clay liners. ASTM D5890-11, ASTM International, West Conshohocken, Pennsylvania, USA
- ASTM. (2014). Standard Test Method for Measuring Mass Per Unit of Geosynthetic Clay Liners. ASTM D5993-14, ASTM International, West Conshohocken, Pennsylvania, USA
- ASTM. (2016). Standard test method for determining the internal and interface shear strength of geosynthetic clay liner by the direct shear method. ASTM D6243/D6243M-16, ASTM International, West Conshohocken, Pennsylvania, USA
- Athanassopoulos, C. and Yuan, Z. (2011). Correlation between needle punch-reinforced geosynthetic clay liner peel strength and internal shear strength. *Geo-Frontiers 2011: Advances in Geotechnical Engineering*, Han, J. & Alzamora, D. E., Editors, ASCE, Reston, VA, USA, GSP No. 211, pp. 1922–1930.
- Berard, J. F. (1997, March). Evaluation of needle-punched geosynthetic clay liners internal friction. In *Proceedings, Geosynthetics*, Vol. 97, pp. 351-362.

- Bouazza, A., Nahlawi, H., and Aylward, M. (2011). In situ temperature monitoring in an organic-waste landfill cell. *Journal of Geotechnical and Geoenvironmental Engineering*, 137(12), 1286-1289.
- Bouazza, A. (2002). Geosynthetic clay liners. *Geotextiles and Geomembranes*, 20(1), 3-17.
- Daniel, D. E., Shan, H. Y., & Anderson, J. D. (1993, March). Effects of partial wetting on the performance of the bentonite component of a geosynthetic clay liner. In *Proceedings of Geosynthetics*, Vol. 93, pp. 1483-1496.
- Duncan, J. M., & Chang, C. Y. (1970). Nonlinear analysis of stress and strain in soils. *Journal of Soil Mechanics & Foundations Division, ASCE*, 96, No. SM5, 1629–1653.
- Eid, H. T., and Stark, T. D. (1997). Shear Behavior of an Unreinforced Geosynthetic Clay Liner. *Geosynthetics International*, 4(6), 645-659.
- Eid, H. T., Stark, T. D. & Doerfler, C. K. (1999). Effect of shear displacement rate on internal shear strength of a reinforced geosynthetic clay liner. *Geosynthetics International*, 6(3) 219–239.
- Fox, P. J., and Stark, T. D. (2004). State-of-the-art report: GCL shear strength and its measurement. *Geosynthetics International*, 11(3), 141-175.
- Fox, P. J., and Ross, J. D. (2011). Relationship between NP GCL Internal and HDPE GMX/NP GCL Interface Shear Strengths. *Journal of Geotechnical and Geoenvironmental Engineering*, 137(8), 743-753.
- Fox, P. J., and Stark, T. D. (2015). State-of-the-art report: GCL shear strength and its measurement—ten-year update. *Geosynthetics International*, 22(1), 3-47.
- Fox, P. J., Rowland, M. G., Scheithe, J. R., Davis, K. L., Supple, M. R., and Crow, C. C. (1997). Design and evaluation of a large direct shear machine for geosynthetic clay liners. *Geotechnical Testing Journal*, 20(3), 279-288.
- Fox, P. J., Rowland, M. G., and Scheithe, J. R. (1998). Internal shear strength of three geosynthetic clay liners. *Journal of Geotechnical and Geoenvironmental Engineering*, 124(10), 933-944.
- Gilbert, R. B., Fernandez, F., and Horsfield, D. W. (1996). Shear strength of reinforced geosynthetic clay liner. *Journal of Geotechnical Engineering*, 122(4), 259-266.
- Gilbert, R. B., Scranton, H. B. and Daniel, D. E. (1997). Shear strength testing for geosynthetic clay liners. *Testing and Acceptance Criteria for Geosynthetic Clay Liners*, STP 1308, Well, L. W., Editor, ASTM International, West Conshohocken, PA, pp. 121–135.

- Giroud, J. P., Darrasse, J. and Bachus, R. C. (1993). Hyperbolic expression for soil-geosynthetic or geosynthetic-geosynthetic interface shear strength. *Geotextiles and Geomembranes*, 12(3), 275–286.
- Gleason, M. H., Daniel, D. E., and Eykholt, G. R. (1997). Calcium and sodium bentonite for hydraulic containment applications. *Journal of Geotechnical and Geoenvironmental Engineering*, 123(5), 438-445.
- Grand View Research (2016). Geosynthetic clay liner market analysis by application (containment and wastewater Treatment, Landfill, Roadways and Civil Construction) and Segment Forecasts To 2022. ISBN Code: 978-1-68038-714-8, <http://www.grandviewresearch.com/>
- Hanson, J. L., Yeşiller, N., and Oettle, N. K. (2009). Spatial and temporal temperature distributions in municipal solid waste landfills. *Journal of Environmental Engineering*, 136(8), 804-814.
- Hornsey, W. P., Scheirs, J., Gates, W. P., and Bouazza, A. (2010). The impact of mining solutions/liquors on geosynthetics. *Geotextiles and Geomembranes*, 28(2), 191-198.
- Hsuan, Y. G. & Koerner, R. M. (2002). Durability and lifetime of polymer fibers with respect to reinforced geosynthetic clay barriers; i.e. reinforced GCLs. *Clay Geosynthetic Barriers*. Zanzinger, H., Koerner, R. M. & Gartung, E., Editors, Swets & Zeitlinger, Lisse, pp. 73–86.
- Koerner, R. M. (1997). Perspectives on Geosynthetic Clay Liners. In *Testing and Acceptance Criteria for Geosynthetic Clay Liners*. ASTM International, West Conshohocken, PA, 3-20.
- Koerner, R. M. (1998). *Designing with Geosynthetics*, 4th ed., Prentice Hall, Upper Saddle River, NJ, 761 pp.
- Koerner, G. R., and Koerner, R. M. (2006). Long-term temperature monitoring of geomembranes at dry and wet landfills. *Geotextiles and Geomembranes*, 24(1), 72-77.
- Lupo, J. F. (2010). Liner system design for heap leach pads. *Geotextiles and Geomembranes*, 28(2), 163-173.
- Martin, J. W., Stark, T. D., Thalhamer, T., Gerbasi-Graf, G. T. and Gortner, R. E. (2013). Detection of aluminum waste reactions and associated waste fires. *Journal of Hazardous, Toxic, and Radioactive Waste*, 17(3), 164–174.
- McCartney, J. S., Zornberg, J. G. and Swan, R. H. Jr. (2009). Analysis of a large database of GCL-geomembrane interface shear strength results. *Journal of Geotechnical and Geoenvironmental Engineering*, 135(2), 209–223.

- Mesri, G. and Olson, R. E. (1970). Shear strength of montmorillonite. *Geotechnique*, 20(3), 261–270.
- Müller, W., Jakob, I., Seeger, S., and Tatzky-Gerth, R. (2008). Long-term shear strength of geosynthetic clay liners. *Geotextiles and Geomembranes*, 26(2), 130-144.
- Olst, J., and Crosson, L. (1999). Geosynthetic clay liner peel index test correlation to direct shear. In *Proc., Sardinia'99, 7th Int. Waste Management and Landfill Symp.* S. Margherita di Pula, Cagliari, Italy.
- Olst, J. T., and Swan Jr, R. H. (2001). Internal shear strength of a geosynthetic clay liner at high normal loads. *Proceedings, Tailings and Mine Wastes '01, Fort Collins, CO*, 197-200.
- Richardson, G. N. (1997). GCL internal shear strength requirements. *Geotechnical fabrics report*, 15, 20-25.
- Rowe, R. K. (2005). Long-term performance of contaminant barrier systems, *Geotechnique*, 55(9), 631-678.
- Shackelford, C. D., Benson, C. H., Katsumi, T., Edil, T. B., and Lin, L. (2000). Evaluating the hydraulic conductivity of GCLs permeated with non-standard liquids. *Geotextiles and Geomembranes*, 18(2), 133-161.
- Shackelford, C. D., Sevick, G. W., and Eykholt, G. R. (2010). Hydraulic conductivity of geosynthetic clay liners to tailings impoundment solutions. *Geotextiles and Geomembranes*, 28(2), 149-162.
- Smith, M. (2008). Emerging issues in heap leaching technology, *EuroGeo4, Proc. 4<sup>th</sup> Geosynthetics Conference*, Edinburgh, Scotland.
- Stark, T. D. and Eid, H. T. (1993). Modified Bromhead Ring Shear Apparatus, *Geotechnical Testing Journal*, ASTM International, West Conshohocken, Pennsylvania, USA. 16(1), pp. 100-107.
- Stark, T. D., and Eid, H. T. (1996). Shear behavior of reinforced geosynthetic clay liners. *Geosynthetics International*, 3(6), 771-786.
- Stark, T. D., Arellano, D., Evans, W. D., Wilson, V. L., and Gonda, J. M. (1998). Unreinforced Geosynthetic Clay Liner Case History. *Geosynthetics International*, 5(5), 521-544.
- Thiel, R., and Smith, M. E. (2004). State of the practice review of heap leach pad design issues. *Geotextiles and Geomembranes*, 22(6), 555-568.

- Thies, M., Gerloff, C., Muller, W. & Seeger, S. (2002). Long-term shear testing of geosynthetic clay liners. *Clay Geosynthetic Barriers*, Zanzinger, H., Koerner, R. M. & Gartung, E., Editors, Swets & Zeitlinger, Lisse, pp. 97–104.
- U.S. Environmental Protection Agency. (1987). *Draft minimum technology guidance for single and double liner systems for landfills and surface impoundments*, Office of Solid Waste, Washington, D.C.
- U.S. Environmental Protection Agency. (1991). *Solid waste disposal facility criteria*. Office of Solid Waste, Washington, D.C.
- U.S. Environmental Protection Agency. (1997). *Geosynthetic Clay Liners Used in Municipal Solid Waste Landfills*. Office of Solid Waste, Washington, D.C.
- von Maubeuge, K. P. and Lucas, S. N. (2002). Peel and shear test comparison and geosynthetic clay liner shear strength correlation. *Clay Geosynthetic Barriers*, Zanzinger, H., Koerner, R. M. and Gartung, E., Editors, Swets & Zeitlinger, Lisse, pp. 105–110.
- Von Maubeuge, K., & Heerten, G. (1994). Needle punched geosynthetic clay liners. In *Proceedings of 8th GRI Conference*, pp. 129-207.
- Zornberg, J. G., McCartney, J. S. and Swan, R. H. Jr. (2005). Analysis of a large database of GCL internal shear strength results. *Journal of Geotechnical and Geoenvironmental Engineering*, 131, (3), 367–380.